HYDROTALCITES AS PHOTOCATALYSTS FOR REDUCTION OF CARBON DIOXIDE

A Project Thesis

Submitted in partial fulfillment of the requirements

For the award of the degree of

MASTER OF TECHNOLOGY

In

CHEMICAL ENGINEERING

SPECIALISATION: CATALYSIS TECHNOLOGY

By

D. SUSHIL KUMAR

(CA10M006)

Under the guidance of

Dr. K. R. Krishnamurthy

Dr. Raghuram Chetty

DEPARTMENT OF CHEMICAL ENGINEERING
INDIAN INSTITUTE OF TECHNOLOGY, MADRAS
CHENNAI – 600 036
MAY, 2012

CERTIFICATE

This is certify that the project report entitled "**HYDROTALCITES AS PHOTOCATALYSTS FOR REDUCTION OF CARBON DIOXIDE"** submitted by **D. SUSHIL KUMAR** (**CA10M006**) to the Indian Institute of Technology, Madras for the award of the degree of Master of Technology in Catalysis Technology, Chemical Engineering is a *bona-fide* record of the work carried out by him under my supervision. The contents of the thesis, in full or parts have not been submitted to any other institute or university for the awards of any degree**.**

Guide

Dr. K.R. Krishnamurthy

National Centre for Catalysis Research

IIT Madras.

Guide

Dr. Raghuram Chetty

Department of Chemical Engineering

IIT Madras.

Chennai – 600 036

Date:

ACKNOWLEDGEMENTS

I am very much grateful to my research guide **Dr. K. R. Krishnamurthy** for his constant encouragement, thought provoking discussions, critical ideas, support, invaluable suggestions and unfailing guidance at every stage of the research programme. It gives me immense pleasure to have been associated with him. I thank him for his patient guidance, open discussions, constant encouragement, unbounded enthusiasm and interest.

I express my sincere gratitude to **Prof. B. Viswanathan** for his inspiring, invaluable guidance, constant encouragement and thought provoking discussions throughout the research work. I am really grateful to him for providing opportunities to learn various aspects in catalysis and photo catalysis. I feel privileged to have been associated with him. It is my privilege to express my gratitude to him for introducing me to the field of catalysis.

I am very much grateful to **Dr. Raghuram Chetty,** my research guide, for his constant encouragement, support and invaluable suggestions and guidance.

I express my deep gratitude to **Prof. S. Pushpavanam**, Head, Department of Chemical Engineering for his support and providing various instrument facilities.

I am thankful to **Mr. JOSEPH** Sir, Workshop Head, Department of Chemical Engineering for Manufacturing the Solar reactor and other faculty members of our department for the support and facilities provided in carrying out this project work.

I sincerely thank all my PG committee members, **Prof. S. Sivasanker**, **Prof. P. Selvam** for their constant encouragement and suggestions. I wish to thank **NCCR** and **IIT Madras** for providing opportunity and all facilities to carry out my project.

I express my heart full thanks to **Ms. V. Jeyalakshmi** for her constant help and support which made it possible for me to complete my work.

I am thankful to **Ms. A. Alagarasi** for surface area analysis, **Mr. Omprakash** for SEM and **Mr. Shankar** for IR analysis. I would like to extend my thanks to the **Head and staff members of CGBS, SAIF** and **Department of Metallurgy** IIT Madras for providing the necessary instrumentation facilities.

I wish to thank my class mates **Mr. Md. Mainak Zaman, Mr. Sunil Mehla** and **Mr. Aditya Ajgaonkar** for their motivation, encouragement and support through out my project period.

I express my sincere thanks to my seniors and colleagues, **Mr. Vamsi Krishna, Mr. Prakash, Mr. Ramana Murthy, Mr. Shanmugam, Mr. Ariharan, Mrs. Renjini, Mrs. Keerthiga, Mr. Kuppan, Mr. Mahendran, Mr. Anil Kumar, Mr. Sudhakar, Mr. Sourav Khan, Mr. Sankaranarayanan, Mr. Ramamohan, Mr. Rajesh Kumar, Mr. Pachamuthu, Ms. Swathi,** and **Ms. Vijayashanthi,** for their kindly help, suggestions and support.

I am deeply indebted to my father, **Sri. D. Shankar** and mother, **Smt. D. Saraswathi** for their constant support and encouragement whenever needed, without them it would have been impossible for me to complete this work.

D. Sushil kumar.

ABSTRACT

KEY WORDS: Photocatalysis, CO_2 reduction, Hydrotalcites, solar energy.

Emission of carbon dioxide into the atmosphere mainly by burning of fossil fuels causes the greenhouse effect or global warming, which is matter of serious concern for the modern society. Tackling this issue has become a major challenge for the scientists and technologists.

One of the best routes to remedy CO_2 is to transform it to hydrocarbons via photo reduction. There by, solar energy is transformed and stored as chemical energy. If hydrogen is not produced through alternative energy methods it does not favor the overall goal of CO_2 mitigation and utilization. This problem can be resolved with catalyst development.

The utilization of solar energy via chemical storage is achieved by photo catalytic or photo-electrochemical activation of light-sensitive catalytic surface. Though Photo-catalytic technology has been emerging as a viable technology for the remediation of pollutants from water, it can be applied to a variety of compounds. One of the factors to be considered is the possibility of mass transfer limitations due to the characteristics imposed in the reaction chamber by the existence of the catalyst in various forms in dispersed state. In fact the construction of a appropriate photo-chemical reactor itself has been a major issue.

The HTLCs itself used as the catalyst since it contains various transition metal cations as the catalytically active species well dispersed on the basic support materials. Thermal decomposition of HTlcs by calcination results in the formation of mixed oxides with a high thermal stability and a large surface area. In addition, well-dispersed metallic particles are obtained after the reduction treatment, leading to different catalytic properties such as, dehydrogenation catalysts, Ni/Mg(Al)O catalysts for the reforming of hydrocarbons, Cu/Zn/Al mixed oxides derived from aurichalcite or HTlcs etc., HTC also function as

efficient photocatalysts for dye-bleaching, removal of organic pollutants from water, splitting of water to yield oxygen.

Changes in terms of substituting divalent and trivalent ions could lead to a number of potentially active catalysts that may display higher activity. Evaluation of catalysts in aqueous phase along with detailed analysis of liquid samples and for hydrogen, oxygen and CO in gas phase are to be carried out to get a complete product profile.

In order to the effect of CO_2: water molar ratio, photoreduction would be carried out in vapor phase, using CO_2 and water vapor in different proportions. In the present case hydrogen generated *in-situ* by photo catalytic water splitting is used. Due to this reason activity observed in the present case is higher, in micromoles/g compared to nano moles /g observed earlier. , CO_2 is employed in excess and CO_2: water mole ration is 1: 0.038. Hence catalyst deactivation is severe due to limited availability of hydrogen via water splitting.

TABLE OF CONTENTS

	Title	Page No
ACKNOWLEDGEMENT		ii
ABSTRACT		iv
LIST OF TABLES		ix
LIST OF FIGURES		x
LIST OF SCHEMES		xii
ABBREVIATIONS		xiii
NOTATIONS		xiv
CHAPTER 1	**INTRODUCTION**	
1.1	Carbon dioxide emission & Green house gas effect.	1
1.2	Activation of Carbon dioxide.	3
1.3	Photo catalysis.	8
1.4	Photo catalytic reduction of carbon dioxide.	8
1.5	Photo catalytic Applications.	11
1.6	Features of catalysts for carbon dioxide reduction.	12
1.7	Catalysts for splitting of water.	12
1.8	Reaction pathways & mechanism for carbon dioxide reduction.	13
1.9	Reduction of carbon dioxide.	14
1.10	Types of catalysts used for CO_2 photo reduction.	15
CHAPTER 2	**HYDROTALCITE**	17
2.1	Hydrotalcite.	17
2.2	Structural features of Hydrotalcites.	18
2.3	Hydrotalcite as the catalysts.	20
2.4	Design of a reactor for CO_2 reduction using sunlight.	21
2.5	Aim and Scope of current investigation.	21
2.6	Experimental approach or work paln	

CHAPTER 3	**EXPERIMENTAL METHODOLOGY**	23
3.1	Chemicals and Materials.	23
3.2	Preparation of Zn-Cu-Al LDH.	23
3.2.1	Preparation of Zn-Cu-Ga LDH.	23
3.2.2	Preparation of Zn-Cu-In LDH.	24
3.2.3	Preparation of (Zn-Ni)-Cu-Al LDH.	24
3.2.4	Preparation of Zn-Cu-(Al-In) LDH.	24
3.2.5	Preparation of Zn-Cu-(Al-Fe) LDH.	25
3.2.6	Preparation of CuO(3 %) loaded TiO_2 (P25) catalyst.	25
3.2.7	Preparation of Ag(7 %) loaded TiO_2 (P25) catalyst.	25
3.3	Techniques for characterization of catalysts	26
3.3.1	X-ray diffraction studies	26
3.3.2	Diffuse reflectance UV-Visible spectrophotometric studies (DRS)	26
3.3.3	Surface area measurements	26
3.3.4	Scanning electron microscopic (SEM) analysis	27
3.3.5	FT-IR Spectroscopic analysis.	27
3.4	CO_2 photoreduction studies	27
	Liquid phase reactor	27
	Analysis of products	28
	Reaction in Vapor phase	29
	Design and construction of Solar Reactor for reduction of Carbon Dioxide	30
CHAPTER 4	**RESULTS & DISCUSSIONS.**	33
4.1	Synthesis and characterization of LDH catalysts.	33
4.1.1	Textural Properties	33
4.1.2	Phase analysis by XRD	33
4.1.3	FT-IR spectra	37
4.1.4	UV-Visible diffuse reflectance spectra	39
4.1.5	Scanning electron microscopy	41

4.2	Evaluation of LDH catalysts for photo catalytic reduction of CO_2 with water (PCR)	43
4.2.1	Evaluation of Zn-Cu-Al in aqueous & vapor phase.	43
4.2.2	Evaluation of all catalysts in vapor phase	46
4.2.3	Evaluation of photo catalysts using solar reactor	48
4.2.4	CO_2 photo reduction on hydrotalcite catalysts	50
CHAPTER 5	**SUMMARY & CONCLUSIONS**	52
	REFERENCES	55

LIST OF TABLES

Table No	Title	Page No
Table 1	Sources of carbon dioxide emission(CO_2)	2
Table 2	Thermodynamics for various reactions involving CO_2	4
Table 3	Types of catalysts used for CO_2 photo reduction	15
Table 4	Textural properties of hydrotalcites	33
Table 5	Crystalline Size & Band Gap data for catalysts	39

LIST OF FIGURES

Figure No	Title	Page No
1	World carbon dioxide (CO_2) emissions in million metric tons of carbon (left) and US CO_2 emissions in thousand metric tons of carbon by fuel type (right).	3
2	Hydrotalcite structure	17
3	Various applications of hydrotalcite.	19
4	XRD pattern for catalyst a) Zn Cu Al	34
5	b) Zn Cu Ga	34
6	c) Zn Cu In	35
7	d) Zn&Ni Cu Al.	35
8	e) Zn Cu Al&In.	35
9	f) Cu Al&Fe.	36
10	IR Spectrum for catalyst a) Zn Cu Al Catalyst	37
11	b) Zn Cu Ga	37
12	c) Zn Cu In.	37
13	d) Zn&NI Cu Al.	37
14	e) ZN Cu Al&In	38
15	f) Zn Cu Al&Fe	38
16	UV spectrum of a) ZnCuAl	39
17	b) Zn Cu Ga	39
18	c) Zn Cu In.	40
19	d) Zn&Ni Cu Al	40
20	e) Zn Cu Al&In.	40
21	f) Zn Cu Al&Fe.	40
22	SEM micrograph & EDAX for catalyst a) Zn Cu Al	41
23	b) Zn Cu Ga	41

24	c) Zn Cu In	42
25	d) Zn Cu Al&In	42
26	Methane formed for both Liquid & vapor Phase.	44
27	Ethane formed for both Liquid & vapor phase.	44
28	Methanol formed for both liquid & Vapor phase.	44
29	Acetaledhyde formed for both Liquid & Vapor phase	45
30	Ethanol formed for both liquid & Vapor phase.	45
31	Methanol formed for ALL catalysts.	46
32	Methane formed for ALL catalysts.	47
33	Ethane formed for ALL catalysts.	47
34	Acetaldehyde formed for ALL catalysts.	47
35	P-25 formed for Solar reactor	49
36	CuO/P-25 formed Solar reactor	49
37	Ag/P-25 formed Solar reactor.	50

LIST OF SCHEMES

Scheme No	Title	Page No
1	Schematic representation of (a) Brucite and (b) Hydrotalcite.	18
2	Set up of photo catalytic reactor for liquid phase.	29
3	Set up of Photo catalytic reactor for vapor phase.	30
4	Set up of solar reactor for both liquid & Vapor phase.	32

ABBREVIATIONS

AR	-	Analytical Reagent
GC	-	Gas Chromatography
FID	-	Flame Ionisation Detector
SEM	-	Scanning electron microscopy
EDS	-	Energy Dispersive Spectra
TPR	-	Temperature Programmed Reduction
TEM	-	Transmission Electron Microscopic
UV-Vis	-	Ultraviolet-Visible
XRD	-	X-ray Diffraction
IR	-	Infra Red
ppm	-	parts per million
Eg	-	Band gap energy

NOTATIONS

eV	-	electron volt
m^2/g	-	Square meter per gram
°C	-	degree celsius
g	-	gram
h	-	hour
nm	-	nano meter
Å	-	Angstrom
λ	-	Wavelength
Wt	-	Weight
θ	-	Bragg's angle
μmol	-	micro mol
ν	-	frequency
W	-	Watt
e^-	-	electron
h^+	-	hole
Φ	-	Work function.

CHAPTER 1

INTRODUCTION

1.1 Carbon dioxide emission & Green house gas effect

Emission of carbon dioxide into the atmosphere mainly by burning of fossil fuels causes the greenhouse effect or global warming, which is matter of serious concern for the modern society. Tackling this issue has become a major challenge for the scientists and technologists.

The sources of CO_2 emissions include stationary, mobile, and natural as listed in Table 1. Anthropogenic emissions include those from energy utilization from mobile and stationary sources, but exclude natural sources (*Etheridge et al., 2008*). Current estimations state that the atmospheric CO_2 concentration is around 384 ppmv and is forecasted to increase at a rate of approximately 1% per annum. Such increases in atmospheric CO_2 are primarily caused by the combustion of fossil fuels for energy consumption (25%) and deforestation (10-30%) (*Xiaoding et al., 1996*). However, it should be mentioned that although CO_2 and other GHG's are suspected to play a role in global climate change, atmospheric CO_2 has an important and positive role in the ecological system, since photosynthesis and food production depend on it as a carbon source. Furthermore, fossil fuels used today originated from atmospheric CO_2 millions of years ago.

Nevertheless, the research conducted in the last five decades, and more notably the last 15 years, shows drastic increase in CO_2 emissions in the last century with a continuing increase at much faster rates than previous years (Fig. 1). As a result of the potential adverse effects of high CO_2 atmospheric concentrations to humans and the environment, a large effort has been put forth to reduce CO_2 emissions from major contributing sources. Several methods for CO_2 mitigation are being investigated:

- CO_2 sequestration;
- Post-treatment capture and utilization (recycle);
- Increase in efficiencies of carbon-based energy systems;

• Use of carbon-free alternative energy sources;

Table1. Sources of carbon dioxide emission (CO_2). (*C. Song et al., 2006*).

Stationary sources	Mobile sources	Natural sources
Fossil fuel-based electrical power plants	Cars, and sport utility vehicles	Humans
Independent power producers	Trucks and buses	Animals
Manufacturing plants in industry[a]	Aircrafts	Plants and animal decay
Commercial residential buildings	Trains and ships	Land emission leakage
Flares of gas at field	Construction vehicles	Volcanoes
Military and government facilities	Military and government devices	Earthquakes

Major concentrated CO_2 sources include plants for manufacturing hydrogen, ammonia, cement, limestone, and soda ash as well as fermentation processes and chemical oxidation processed.

When examining methods for CO_2 mitigation, the process should be efficient and should not require substantial energy input from conventional energy systems (e.g. fossil fuel power generation). Sequestration of CO_2 in geological formations such as deep-sea beds or use in enhancing fossil fuel recovery is a highly debated method. The ability for such systems to handle billions of tons per year is still unanswered. Moreover, the processes for sequestration requires large energy input, which in turn leads to more GHG emissions if supplied by conventional power generation methods.

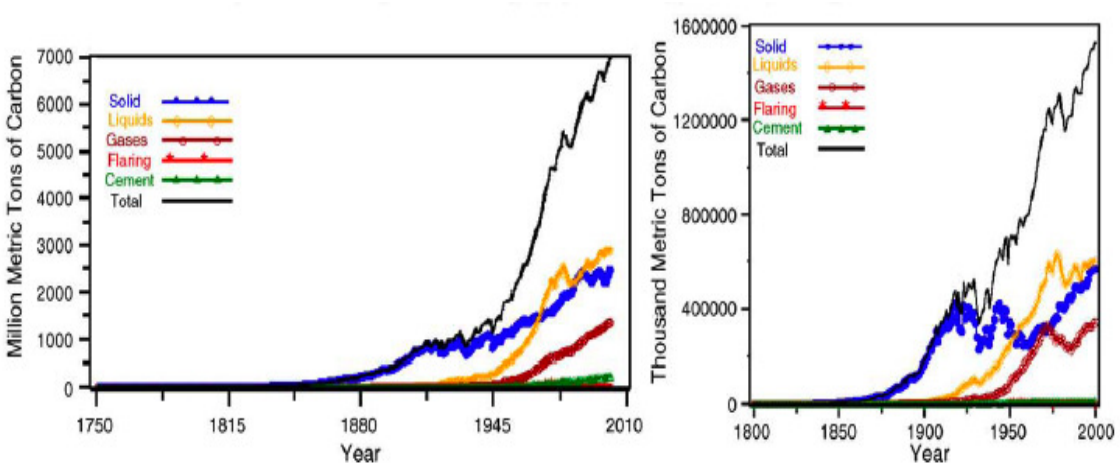

Fig 1. World carbon dioxide (CO_2) emissions in million metric tons of carbon (left) and US CO_2 emissions in thousand metric tons of carbon by fuel type (right). Taken from (*Marland et al., 2005*).

The increase in efficiencies of carbon-based energy systems will help to reduce future emissions; however, it does not supply an avenue to reduce existing CO_2 atmospheric concentrations. On the other hand, implementing carbon-free alternative energy sources requires significant socio-economic changes. These methods raise many political, environmental, and economic concerns.

Conversely, converting or recycling CO_2 into value-added products, such as high-energy content fuels like methanol, suitable for utilization in existing infrastructure appears to be an attractive option. The first step in any such process aimed at CO_2 conversion to useful chemicals is the activation of carbon dioxide.

1.2 *Activation of CO_2*

Carbon dioxide is a colorless, odorless, and a relatively inert gas. As a linear molecule with a double bond between the carbon and oxygen atoms (O = C = O) there is no dipole moment. In nature, CO_2 serves as a carbon source for the photosynthesis of organic compounds. Natural photosynthesis in plants occurs through several steps involving dark and light reactions to generate carbohydrates and oxygen from abundant raw reactants, CO_2

and H_2O (*Walther et al., 1999*). Over the past twenty years, a great deal of effort has been devoted to understand and mimic the mechanism of the light reactions in photosynthesis in which light energy is transformed into chemical energy. During this process, activation of CO_2 is achieved through a chain of electron carriers and chromophores. The work of *Collin et al., 1994* and *Balzani et al., 1996* cover artificial photosynthesis from the point of view of energy transfer and charge separation in multiple-component systems with transitional metal complexes.

Although such homogeneous and micro heterogeneous systems have shown to reduced product of CO_2/mol catalyst), low yields of only single carbon products, and the lifetime along with the selectivity of single components is not well understood. Moreover, such studies focus on homogeneous metal complexes, which can be expensive and are not practical for large-scale purposes. Thus the question arises, why is it so difficult to mimic nature and is it really possible? To answer such questions, a closer examination of thermodynamics and the bonding orbitals of CO_2 are required.

Being the most abundant and oxidized form of carbon occurring in nature, it is also one of the most stable of carbon compounds. A strong indication of a CO_2 molecule's stability can thermodynamically be inferred by its large, negative standard Gibbs free energy of formation value ($\Delta_f G^0$ = -349.67 kJ mol^{-1}) (*R.H. Perry's et al, 2008*). Given that CO_2 is such a stable compound, consequently a substantial input of energy or a high-energy substrate is required for chemical conversion.

This problem can be resolved with catalyst development; however, an important consideration for feasibility is a close examination of the thermodynamics of such reactions as shown in Table2.

Table 2. Thermodynamics for various reactions involving CO_2. (*Surf et a1.,1996)*

Reaction	ΔH^0(kJ mol^{-1})	ΔG^0 (kJ mol^{-1})	Eqn. #
$CO_{2(g)} + H_{2(g)} \rightarrow CO_{(g)} + H_2O_{(g)}$	41.2	18.6	(3)
$CO_{2(g)} + H_{2(g)} \rightarrow CO_{(g)} + H_2O_{(l)}$	-2.8	20.0	(4)

$CO_{2(g)} + H_{2(g)} \rightarrow HCOOH_{(l)}$	-31.2	33.0	(5)
$CO_{2(g)} + 2H_{2(g)} \rightarrow CHOH_{(l)} + H_2O_{(l)}$	-9.0	44.0	(6)
$CO_{2(g)} + 3H_{2(g)} \rightarrow CH_3OH_{(l)} + H_2O_{(l)}$	-131.3	-9.2	(7)
$CO_{2(g)} + 4H_{2(g)} \rightarrow CH_{4(g)} + 2H_2O_{(l)}$	-252.9	-130.8	(8)
$2CO_{2(g)} + 6H_{2(g)} \rightarrow CH_3OCH_{3(l)} + 3H_2O_{(l)}$	-264.9	-38.0	(9)

When first examining Table 2, it is noted that several of the reactions involving CO_2 are exothermic in light of the stability of the CO_2 molecule. It is worth mentioning that endothermic reactions, such as Eqn. 4 among several others, can be feasible and indeed useful. For example, some industrial endothermic reactions used today on large-scale are thermal cracking of hydrocarbons, dehydrogenation reaction of ethylbenzene to make styrene, and steam reforming for producing synthesis gas. Nevertheless, chemical reactions are driven by the difference in Gibbs free energy of products and reactants as shown by Eqn. 10. It is clear that most of the reactions in Table 4 have positive ΔG^0 values and thus are not thermodynamically favored.

$$\Delta G = \Delta H - T\Delta S \qquad (10)$$

For values in Table 2 where $\Delta G^0 < 0$, they correspond to hydrogenation reaction, leading to products containing C-O, for the most part. A reason for the relatively favorable values of ΔG^0 for hydrogenation is that water is produced. However, it is important to note that these values involve the use of hydrogen. The hydrogen has to either be supplied by an outside source or via water splitting reaction in which both cases present their respective problems.

For the latter case, the competition between electrons for water splitting for hydrogen production and for CO_2 reduction arises in aqueous medium resulting in lower conversions and efficiencies. For the former case, if hydrogen is not produced through alternative energy methods it does not favor the overall goal of CO_2 mitigation and utilization.

There are variety techniques under the investigation for CO_2 conversion such as

Radiochemical

$$CO_2 \xrightarrow{\gamma-radiation} HCOOH, HCHO$$

Chemical reduction

$$2Mg^{2+} + CO_2 \longrightarrow 2MgO + C$$

$$Sn^{4+} + 2CO_2 \longrightarrow SnO_2 + 2CO$$

$$2Na^{+} + 2CO_2 \longrightarrow Na_2C_2O_4$$

Thermo chemical

$$CO_2 \xrightarrow{Ce^{4+}+h\nu} CO + \tfrac{1}{2} O_2 \ (T > 900^{o}C)$$

Photochemical

$$CO_2 \xrightarrow{h\nu} CO, HCHO, HCOOH$$

Electrochemical

$$CO_2 + xe^{-} + xH^{+} \longrightarrow CO, HCOOH, (COOH)_2$$

Biochemical

$$CO_2 + 4H_2 \xrightarrow{bacteria} CH_4 + 2H_2O$$

Photo-electrochemical

$$CO_2 + 2e^{-} + 2H^{+} \xrightarrow{h\nu} CO + H_2O$$

Bioelectrochemical

$$CO_2 + \text{oxoglutaric acid} \xrightarrow{enzyme+methylvio\log en} \text{isocitric acid}$$

Biophotoelectrochemical

$$CO_2 \xrightarrow{h\nu+enzyme+methlyvio\log en+p-\ln P} HCOOH$$

Because the CO_2 reduction process is thermodynamically uphill, we convert carbon dioxide (CO2) to produce fuels using renewable energy (solar energy) and are used as energy source, which has the potential to reduce CO2 emissions, and lower the consumption of fossil fuels.

Water and carbon dioxide splitting processes take place simultaneously on the photo catalyst/co-catalyst surface, and thermodynamic requirements of these processes put constraints on the band gap of the materials used as photo catalysts. Hydrogen formation from water involves a free energy change (ΔG^0) of 237kJ/mol and an enthalpy change (ΔH^0) of 285 kJ/mol; the corresponding values for CO formation from CO_2 are 257 and 283 kJ/mol at 25 °C (1 atm). Hence, the minimum energy required for water and CO_2 splitting processes are, respectively, 1.229 and 1.33 eV (per photon). In theory, the band gap of a photo catalyst used for co-splitting of CO_2 and water should be at least 1.33 eV.

In order to develop a process that is not only *green* but also is able to address some of the aforementioned limitations, the energy required for the reduction process preferably should be supplied by renewable and/or alternative sources. One such avenue, which still requires a more in-depth study, is the photo-electrochemical and photo-catalytic reduction of CO_2 to simple alcohols and low chain hydrocarbon fuels. Photo-electrochemical and photo-catalytic reduction of CO_2 are very similar in that a large portion (photo-electrochemical) to all (photo-catalytic) the energy required for the reduction is supplied by solar irradiation rather than external source (e.g., fossil fuel power plant).

Several studies have reported converting CO_2 into various forms such as carbon monoxide (Suzuki et al, 1985), formaldehyde(*Srinivasan et al., 1977*), formic acid (*Bandi et al*, *1990*), methanol (*Schwartz et al., 1993*), ethanol (*Bandi et al.*, *1992)*, n-propanol (*Schwartz et al.*, 1993), methane(*Suzuki et al*, *1985*), ethane and ethylene (*Hara et al*, *1995*). Although several reports indicate high Faradaic efficiencies (~95%) with electrochemical reduction of CO_2 to such fuels, there are still limitations within such systems, mainly owning to:

• kinetic limitations due to low solubility of CO_2 in water;

• competition with hydrogen evolution reaction in aqueous solutions;

• high-energy demand for conversion;

• uncontrolled intermediates.

The utilization of solar energy via chemical storage is achieved by photo catalytic or photo-electrochemical activation of light-sensitive catalytic surface. From these two systems, photo catalytic system is the best, because it is easy and simpler to construct.

1.3 *Photo catalysis*

Photo catalysis is the acceleration of a photo reaction in the presence of a catalyst (*Fujishimaa et al., 2007*). In catalyzed photolysis, light is absorbed by an adsorbed substrate. Photo induced reactions are activated by absorption of a photon with sufficient energy, i.e., equal or higher than the band-gap energy (*E*bg) of the catalyst. The absorption leads to a charge separation due to the promotion of an electron (e−) from the valence band of the semiconductor catalyst to the conduction band thus generating a hole (h+) in the valence band. In order to have a photo catalyzed reaction, the e−–h+ recombination, subsequent to the initial charge separation, must be prevented as much as possible.

Photocatalysis is the process by which absorbed light is used to drive a chemical transformation aided by a catalyst. The catalyst can either absorb the light itself or harness the light absorbed by another molecule. Efficient solar fuel generation requires efficient (1) light absorption, (2) charge separation, and (3) use of the separated charges in fuel-forming reactions. These reactions must produce the desired fuel (e.g., H2, CH3OH) and a desirable co-product (e.g. O2 from water oxidation).

1.4 *Photo catalytic reduction of CO_2*

The photo-catalytic activation and reduction of CO_2 has been attempted in a number of ways using suitable catalysts, sensitizers, transfer and sacrificial agents in both homogeneous and heterogeneous systems. These recent studies have introduced the photo-reduction of CO_2 as a potential application to convert to fuels such as methane, methanol,

ethanol, and formic acid. An important feature of the photo-electrochemical reduction of CO_2 is not only the utilization of process-waste CO_2 streams as a fuel source, but such systems utilize the most abundant sources of energy and hydrogen, being sunlight and water, respectively. Solar photo-electrochemical and photo-catalytic reduction to produce fuels by use of water as the hydrogen source thus has the potential to be a means to store intermittent solar energy and recycle CO_2 while decreasing the use of fossil fuels, and in turn harmful GHG emissions. Despite recent advancements in the field of photo-electrochemistry and photo-catalysis with regard to CO_2 conversion, yields are quite low and still warrant a comprehensive investigation.

A study of CO_2 photo-catalysis in the absence of a reductant was performed by *Kaneco and coworkers.* A suspension of titania powder in supercritical CO_2 was illuminated by a Xe lamp. Following the irradiation, degassed aqueous solution was added to protonate the reaction intermediates on the titania powder. The results showed that CO_2 molecules interact with the excited-state photo-catalyst surface, resulting in the formation of $CO_2^{\bullet-}$ radicals. During irradiation, no gaseous reduction products were identified. It was inferred that the $CO_2^{\bullet-}$ anion radicals cannot be adsorbed on another $CO_2^{\bullet-}$anion radical, because the excited surface of the photo-catalyst is more active than the $CO_2^{\bullet-}$ radical. However, following a washing process with several solvents, formic acid was detected. From these studies, it was noted that the amount of H^+ in the reductant controls the direction and selectivity of the CO_2 photo-reduction products and the amount of formic acid increased with the pH of the solution.

Improving the efficiency in aqueous systems using sacrificial electron donors such as trimethylamine, triethanolamine, dimethyformamide and isopropyl alcohol has also been extensively studied. Beyond the use of water as a reductant, CO_2 photo-catalysis can be achieved in the presence of gas-phase H_2S, H_2, and CH_4. The use of hydrogen as an alternative for photo-catalytic reduction of CO_2 has also been investigated. The primary products were found to be CO. Although CO may be toxic it serves as a valuable substrate for many industrial processes, such as Fischer-Tropsh synthesis or methanol synthesis. The first step in CO formation produces formate from CO_2 and H_2. The second is the reduction of CO_2 to CO on the formate radical.

For solar fuel production to be economically and environmentally attractive, the fuels must be formed from abundant, inexpensive raw materials such as water or CO2. The thermodynamics for generation of fuels such as H_2, CH_3OH, or CH_4 by photo decomposition of water or CO2 in aqueous solutions.

There are two conceptual routes to produce renewable Carbon containing fuels using solar energy.

- The direct photo reduction of CO_2 using water as a reductant.
- The photolysis of water to generate hydrogen and further reaction of this hydrogen with carbon dioxide forming C_1–C_2 fuels.

For Homogeneous catalytic CO_2 reduction, mostly transition metal complexes (e.g., containing Ru and Ir) as catalysts used for photo reduction of CO2 because they absorb a significant part of the solar spectrum, have long-lived excited states, and can transfer electrons to from small molecules. All water oxidation catalysts based on transition metals and thermodynamic requirements of these processes put constraints on the band gap of the materials and have oxidation states accessible in the 1-1.5v range (17). Few systems include a secondary metal complex (e.g., containing Co) as a co-catalyst to carry out the reduction of CO_2. Metal hydride complexes are also important because bimolecular reactions of hydrides or their reactions with H_2O/H_3O+ are responsible for the formation of H_2.

The rate of a photo catalytic reaction especially depends on the type of the photo catalytic semi conductor and on the light radiation that it used in its initiation.
Further factors that influence a photo catalytic reaction are:

- pH of the medium with which the semiconductor surface is in contact;
- concentration of the substrate influencing the reaction kinetics;
- stream of photons, as oversupply of light accelerates electron–hole recombination;

- Higher temperatures cause frequent collision between the semiconductor and the substrate.

1.5 ***Applications of photocatalysis:***

Photo catalysis provides a number of attractive features:

- A wide variety of compounds may undergo selective redox transformations, decompose, or be deposited;
- It operates at near ambient temperature;
- It utilizes solar energy.

A number of research topics in photo catalysis have emerged that offer potential for commercial development of particular promise are the following subjects:

- selective synthesis of organic compounds;
- removal of organic pollutants;
- removal of inorganic pollutants;
- photo killing of pathogenic organisms (viruses, bacteria, algae protozoa and cancer cells);
- self-cleaning and anti-fogging materials.

Heterogeneous photo catalytical reactions can be carried out either in aqueous solution or gas phase.

According to DOE report, generation of solar fuels raises some of the most challenging fundamental questions in chemistry, materials science, and molecular biology: Can we develop effective catalysts that can take separated charges — regardless of whether they are produced from solar electric photovoltaic (PV) cells or from molecule-based, light-absorbing assemblies — and convert those electrical charges into chemical fuels efficiently and without excessive energy losses during the process?

1.6 ***Features of catalysts for CO_2 photo reduction:***

- CO_2 photo reduction process is highly complex, involving multi electron transfer and non-selective, leading to a range (C_1-C_3) of hydrocarbon products.
- Design of catalysts, consisting of photo catalysts and co-catalysts aided by metal ion / anion doping and light harvesting components/sensitizers, is equally complex.
- Ideal catalysts are expected to display maximum efficiency towards solar energy absorption and possess requisite band energy level characteristics to drive the redox reactions.
- The process involves two steps, splitting of water and reduction of carbon dioxide, which is thermodynamically more favorable. Since the second step involves multi-electron transfer, the rates are very slow relative to the first. These two steps are to be synchronized to achieve higher yields of hydrocarbons.

Inoue *et al., 1979.* Is first to report the photo catalytic reduction of CO_2 in aqueous solutions to produce a mixture of formaldehyde, formic acid, methanol and methane using various wide-band-gap semiconductors.

1.7 ***Catalysts for splitting of water:***

First catalyst for splitting of water was discovered by *Fujishima* and *Honda*, based on TiO_2 and Pt in 1972. Today over 130 inorganic materials have been discovered as catalysts for this reaction. Photochemical splitting of water into H_2 and O_2 using solar energy is a process of great economic and environmental interest.

At a power level of 1000 W/m^2, the solar energy incident on the earth's surface exceeds all human energy needs. A photovoltaic and electrochemical solar cell convert's solar energy into electricity reaches up to 55–77% efficiency, but remain uneconomical because of high fabrication costs, insufficient light absorption, and inefficient charge transfer. In the process photosynthesis, solar energy can also be used to convert water into H_2 and O_2, the fuels of a H_2-based energy economy.

$$H_2O \rightarrow \tfrac{1}{2}O_2(\Delta) + H_2(g); \quad \Delta G = +237\ \text{kJ/mol}$$
$$(1.3\ \text{eV/e}, \lambda\text{min} = 1100\ \text{nm}) \quad \textbf{(11)}$$

Reaction 11 is catalyzed by many inorganic semiconductors. Today, over 130 materials and derivatives are known to either catalyze the overall splitting of water according to eqn. 11 or cause water oxidation or reduction in the presence of external redox agents.

1.8 *Reaction pathways & mechanism for CO_2 photo reduction*

Based on the detailed mechanistic studies on typical TiO_2 catalysts, the following elementary steps could be envisaged:

1. Absorption of light energy by photo catalyst and generation of electron-hole pairs.
2. Charge separation, retarding re-combination and trapping of charge carriers by photo catalyst & co-catalyst.
3. Reduction of water leading to surface H & OH species and stepwise reduction of CO_2 to CO and further to surface C species, both processes taking place on Ti^{3+} sites (formed by photo-generated electrons).
4. Surface transformations via multiple electron transfer, hydrogenation of surface carbon, resulting in the formation of methane, methanol etc involving both Titania & co-catalyst sites.

These transformations represented on a typical TiO_2 surface are schematically shown below along with respective reduction potentials (*Indrakanti et al.,* 2009 & *Fujishima et al.,* 2005).

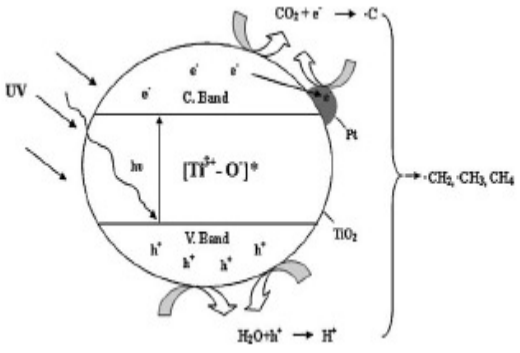

Reaction	E^0_{redox}, V vs. NHE
$2H^+ + 2e^- \rightarrow H_2$	-0.41
$H_2O \rightarrow 1/2O_2 + 2H^+ + 2e^-$	0.82
$CO_2 + e^- \rightarrow CO_2^{\cdot-}$	-1.90
$CO_2 + H^+ + 2e^- \rightarrow HCO_2^-$	-0.49
$CO_2 + 2H^+ + 2e^- \rightarrow CO + H_2O$	-0.53
$CO_2 + 4H^+ + 4e^- \rightarrow HCHO + H_2O$	-0.48
$CO_2 + 6H^+ + 6e^- \rightarrow CH_3OH + H_2O$	-0.38
$CO_2 + 8H^+ + 8e^- \rightarrow CH_4 + 2H_2O$	-0.24

.

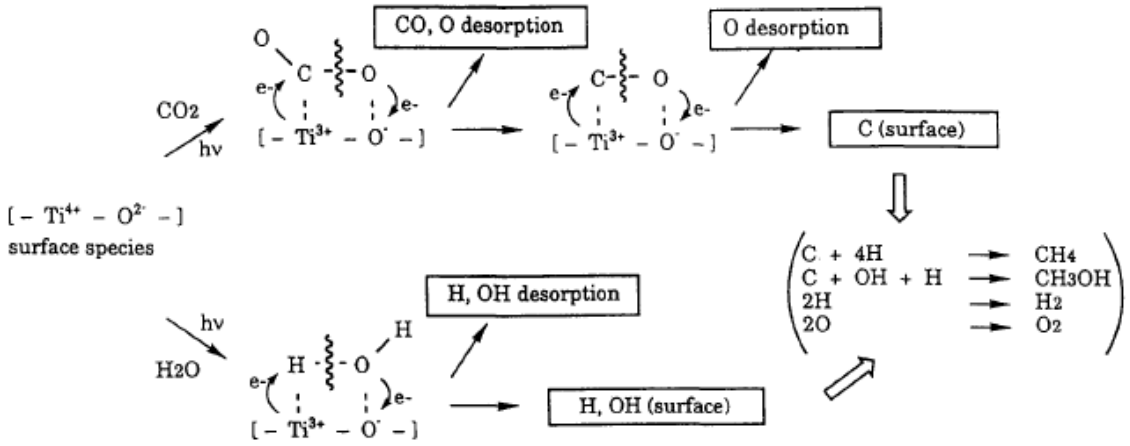

Transient surface species like Ti^{3+}, surface carbon, carbonate, formate, & methoxy radicals have been identified by spectroscopic techniques under different conditions (*Wu et al., 2009*). However, details of charge transfer between semi-conductor- co-catalyst- surface species & electronic features of the interface are yet to be understood in clear terms.

Of the two major steps, photo-reduction of CO_2 is favored thermodynamically over the water splitting. However, water splitting is kinetically fast since it involves four electron transfer while CO_2 reduction eight electrons.

1.9 *Reduction of carbon dioxide:*

The reduction of CO_2 emissions can be achieved by three approaches (*Usubharatana et al., 2006*):

(1) Efficient use of carbon-based energy sources,

(2) Use of alternative or carbon-free energy sources,

(3) Use of a post treatment carbon-capture technology.

Carbon capture refers to the removal of CO_2 from industrial flue gas by a gas separation process prior to release to the atmosphere.

1.10 ***Types of catalysts used for CO_2 photo reduction:***

Table 3:

Light source	**catalyst**	**Reaction medium**	**products**	**efficiency**	**references**
Natural sunlight through solar concentrator	$SrTiO_3$	Aqueous suspension	Formic acid, formaldehyde, methanol	η =0.011%	Halmann et.al., ref 22
UV Xe lamp	SiC and other semiconduc-ting powders	EC cell	Methanol, formic acid, formaldehyde, methane		Inove et.al., ref 23
UV 365 nm	Cu added p-SiC	$KHCO_3$ solution	Methane, ethane & ethylene		Cook et al., ref 24
UV Xe lamp	Cu added TiO_2	Aqueous suspension with pressurized CO_2	Methane, ethylene		Adachi et al., ref 25
UV Hg lamp	TiO_2 loaded Zeolite	CO_2 and H_2O vapor	methanol		Anpo et al., ref 26
UV Hg lamp	Cu added ZrO_2	$NaHCO_3$ solution	CO		Sayama and Arakawa, ref 27
UV Hg lamp	Ti containing SiO_2 film	CO_2 and H_2O vapor	Methane and methanol	QE =0.28%	lkeve et al., ref 28
UV lamp	TiO_2 powder	CO_2 and H_2O vapor	Methane, hydrogen, CO		Tan et al., ref 29

UV lamp	TiO_2(Degussa,P25), ZrO_2	$H_2 + H_2O$	Methane, Ethane, CO		Lo et al., ref 30
UV 365 nm	MW-CNT supported TiO_2	CO_2 and H_2O vapor	Ethanol, formic acid		Xia et al., ref 31
UV 365 nm	Ag/Cu-TiO_2 coated optical fiber	CO_2 and H_2O vapor	methanol	QE = 0.00013%	Wu et al., ref 32
UV 310-435 nm	Ru/RuO_x sensitized TiO_2	CO_2, H_2 in Ar	methane		Thampi et al., ref 33
Visible light $\lambda > 400$nm	Ru-bipyridine-Co(ll) chloride	Acetonitrile / water/ triethyleamine	CO		Lehn and Ziessel.ref 34
Natural sunlight of AM 1.5 illumination	Cu, Pt cocatalyzed N- doped TiO_2 nanotube arrays	CO_2 and H_2O vapor	Methane, other alkanes, olefins, Br-paraffins, H_2, CO	η=0.0148% QE= 0.74%	Varghese et al., ref 35
Visible light $\lambda > 420$ nm	CdSe/Pt/ TiO_2 Heterostruct-ure	CO_2 and H_2O vapor	Methane, methanol, CO, H_2		Wang et al., ref 36

Though several catalyst systems have been investigated, there exists ample scope to improve the overall conversion of CO_2 and achieve desirable product pattern. Thus the search for more efficient catalysts is still on. In this context, hydrotalcite based materials with interesting structural and photophysical properties appear to be promising and worth exploring.

CHAPTER 2
HYDROTALCITES

2.1 *Hydrotalcites:*

Hydrotalcite, magnesium-aluminum hydroxycarbonate, is a naturally occurring mineral of the chemical composition $Mg_6Al_2(OH)_{16}CO_3{\times}4H_2O$. This mineral exhibits a layered crystal structure similar to that of brucite, $Mg(OH)_2$, where each Mg^{2+} cat ion is octahedrally surrounded by six hydroxyl groups and the adjacent octahedra share edges to form infinite sheets. The sheets are stacked one on top of the other and are held together by hydrogen bonding. In hydroxide sheets of hydrotalcite, an Mg^{2+} /Al^{3+} isomorphous substitution in the octahedral sites results in a net positive charge neutralized by interlayer an ionic species (*Kannan et al*, 2006).

General formula:

$$[M^{II}_{1-x}M^{III}_{x}(OH)_2]^{x+}[A^{n-}_{x/n}\cdot yH_2O]^{x-}$$

where M^{II} and M^{III} are divalent and trivalent metal cations, A^{n-} is n- valent an ion and x varies usually between 0.20 and 0.35.

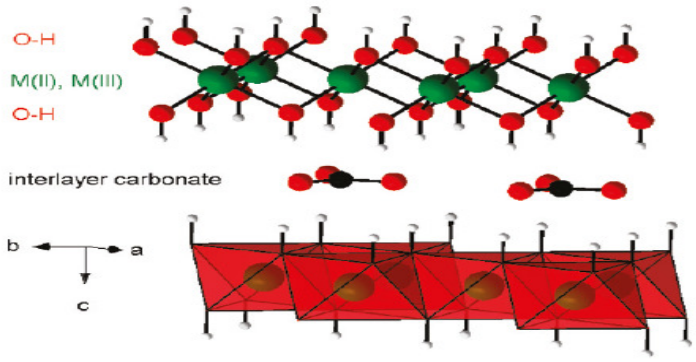

Fig 2: Hydrotalcite-like compounds exhibit positively charged brucitic (MII, MIII)$(OH)_2$ layers, which are built from edge-sharing octahedra, and charge compensating interlayer anions. Here, a couple of adjacent layers and two possible positions for the carbonate anions in the interlayer space are shown. Interlayer water molecules are not shown for clarity (*Lang et al*, 2008).

2.2 ***Structural features of HTlcs:***

The structure of these HT-like materials is visualized by starting with the structure of brucite (Scheme 1a). In brucite structure, Mg^{2+} is surrounded by six hydroxyl groups in an octahedral co-ordination and these octahedra are connected through edge sharing to form infinite sheets. These infinite sheets are stacked upon one another to give layered network held through hydrogen bonding. If one of the Mg^{2+} ions is substituted by a trivalent cation, having a similar ionic radius, like Al^{3+} (in hydrotalcite) (Scheme 1b), the positive charge density of the layer increases. To maintain the electric neutrality, the anions occupy the interlayer positions where water of crystallization also finds a place. These sheets containing both di- and tripositive cations occupy randomly in the octahedral holes of the close packed configuration of hydroxyl ions and the interlayer constituents namely the anion and water are randomly located in this region and possess a high degree of mobility. The wide maneuverability of bivalent ions, trivalent ions, anions in inter layers with varied compositions assist in the design of a large class of isostructural materials with varied physicochemical properties which in turn on the catalytic behavior (*Rowan et al., 2009*).

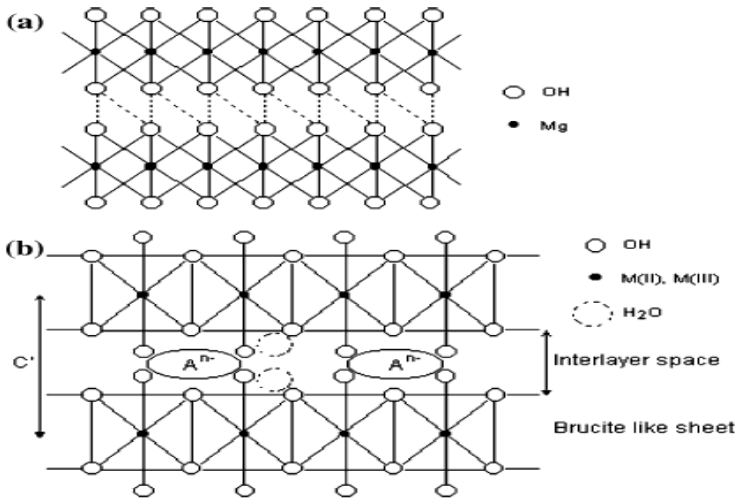

Scheme 1: Schematic representation of (a) Brucite and (b) Hydrotalcite.

2.3 ***HTLCs as the catalysts:***

The HTLCs itself used as the catalyst since it contains various transition metal cations as the catalytically active species well dispersed on the basic support materials. Also used as catalysts mainly after the calcination since the oxides obtained by calcination possess interesting properties such as high surface area and basic properties. After the calcination,

homogeneous mixtures of oxides are formed with very small crystal size, stable to thermal treatments, which further form small and thermally stable metal crystallites by reduction. Moreover, the calcined oxides show a unique property, i.e., ‘‘memory effect’’, which allows the reconstitution of the original HT structure contacting the oxides after the calcination with aqueous solutions containing various anions (*Takehiraa et al., 2007*).

HTLCs possess the structure basically composed of brucite -like layers and anions; various metal cations or metal-containing anions can be incorporated as far as ionic radii and valence state are permitted. These metal species are randomly distributed in the brucite phase and possibly show the catalytic activity for various types of reaction being assisted by the HT structure.

By adopting the ‘‘memory effect’’, HT structure was reconstituted in the mixed oxide derived from the hydrotalcite. Such hydrotalcites reconstituted finely modify the surface of mixed oxides and also showed a unique catalytic activity in the oxidation reactions.

Thermal decomposition of HTlcs by calcination results in the formation of mixed oxides with a high thermal stability and a large surface area. In addition, well-dispersed metallic particles are obtained after the reduction treatment. Moreover the structure can accommodate a wide variation of the different metals, leading to different catalytic properties such as, dehydrogenation catalysts, Ni/Mg(Al)O catalysts for the reforming of hydrocarbons, Cu/Zn/Al mixed oxides derived from aurichalcite or HTlcs etc.,

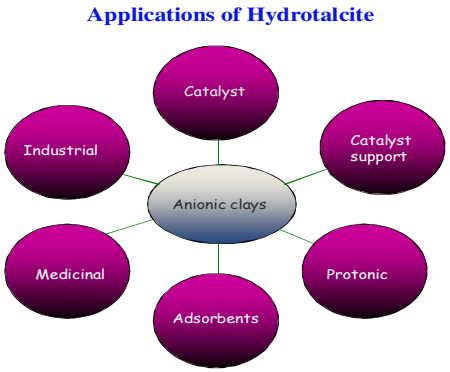

Fig 3: Various applications of hydrotalcite.

Hydrotacites as catalysts or supports are used extensively for various processes like, slective oxidation of alcohols and volatile organic compounds, hydroxylation of phenol & benzene, isomerization of alkenes, dehydrogenation and reforming of hydrocarbons, methanol steam reforming, esterification of acids and a basic catalysts for aldol type condensation. HTC also function as efficient photocatalysts for dye-bleaching, removal of organic pollutants from water, splitting of water to yield oxygen.

2.4 *Design of a reactor for CO_2 reduction using sunlight*

Most of the photo catalytic processes require the use of photo reactor, a device which brings photons, a photo catalyst and reactants into contact, as well as collecting the reaction products.

The solar photo reactor design systems which are most applicable for industrial scale implementation are:

Parabolic trough, compound parabolic, inclined plate, double skin sheet, rotating disk, water bell, fiber optic, and fixed/fluidized bed photo reactors.

- Compound parabolic photo reactors are most suited to near term applications at pilot-scale and well-known design methodology.
- Double-skin sheet photo reactors are also suited to near term applications; significantly less is known about the design and performance.
- Compared to other photo reactor designs, the simplified design and low material cost of inclined plate photo reactors makes them particularly suitable for use in economically and logistically challenged areas where the volumes to be treated are small.
- Fluidized bed photo reactors are highly efficient, but more research is needed to design and operation, for effective use with solar radiation.
- The other photo reactor designs are unlikely to use due to high mechanical complexity, poor efficiency, and/or susceptibility to environmental conditions but may find limited use in specialized applications, e.g. in instances where it is advantageous to separate the light gathering and photo catalytic components of the photo reactor.

2.5 *Aim and scope of the current investigation*

The objective of the current investigation is twofold:

a) To explore the use of hydrotalcite (layered double hydroxides (LDH)) based materials as catalysts for CO_2 photo reduction.
b) To establish a lab-scale solar reactor using direct sunlight for photo catalytic conversion.

The following characteristics of HTLCs make them an interesting class of materials for photocatalysis in general and photocatalytic reduction of CO_2 in particular.

- Possess sufficient capacity to adsorb and activate CO_2.
- Good semi-conductors with band energy corresponding to UV-Visible range.
- Variety of divalent (CO, Ni, Cu, Zn Mg) as well as trivalent (Al, Cr, Ga, In, Fe) ions can be introduced into the layered structure resulting in spectrum of photophysical and catalytic properties. These ions are capable of bringing out a wide range of redox conversions with photo generated charge carriers.
- Carbonate ions in the inter layers can take part in the reaction, providing another route for activation of gas phase CO_2.
- Basic moieties and metal complexes can be introduced into the interlayer's via pillaring effect thus providing yet another mode of activation.
  - Such pillaring would increase the interlayer gap, improving molecular diffusion during reaction.

2.6 *Experimental approach/work plan*

Based on the points discussed above it is proposed to investigate the following aspects:

A. Peparation characterization and performance evaluation of a series of HTLC based catalysts like:

a.(Zn,Cu)- M(III) layered double hydroxides, with M= Al, Ga & In Optimum composition of the metal ions would be fixed based on the literature data and the expected photo-physical properties.

b. Effect of addition of metal promoters Pt, Ru, Au & Ag to the HTLC materials.

B. Designing a solar photo reactor with suitable solar radiation collectors and conducting experiment under direct sunlight using selected HTLC materials.

C. Initial studies are to be performed in laboratory with thermostatic glass reactor, where in catalyst particles are dispersed in water with continuous stirring and irradiated with UV-VIS lamp. Water is saturated with continuous flow of CO_2 and reaction is carried out in batch mode.

D. In order to study the effect of CO_2: water molar ratio, photoreduction would be carried out in vapor phase, using CO_2 and water vapor in different proportions.

E. The CO_2 photoreduction is carried out under direct sunlight using solar reactor for the prepared catalysts Cu/TiO_2 & Ag/TiO_2.

CHAPTER 3

EXPERIMENTAL METHODOLOGY

3.1 *Chemicals and materials:*

For the synthesis of LDH compounds, zinc nitrate hexahydrate (Wako Pure Chemical, >99%), copper nitrate trihydrate (Wako Pure Chemical, >99%), gallium nitrate hydrate (Wako Pure Chemical,>99.9%; n=7–9 of $Ga(NO_3)_3.nH2O$), aluminum nitrate nonahydrate (Wako Pure Chemical, >99.9%), Indium nitrate hydrate (Wako pure chemical ,>99%),sodium carbonate (Wako Pure Chemical, >99.8%), and sodium hydroxide (Kanto Chemical,>97.0%) are used. Deionized water (<1.0 μS cm^{-1}) was used throughout the syntheses.

3.2 *Preparation of Zn-Cu-Al LDH:* (*Ahmed et al*., *2011*).

A mixture of 20 ml solution of each Zinc nitrate hexahydrate of 0.375M, Copper nitrate trihydrate of 0.375M and Aluminium nitrate nonahydrate of 0.25M is dropped at the rate of 0.6ml/min into 100 ml of a 0.075 M Sodium carbonate solution in a flask, with continuous mixing at a rate of 300 rpm. The pH was maintained at 8 by adding 1.0 M sodium hydroxide. After the complete addition, the mixture was continuously stirred at the same rate at room temperature for 2 h. Then the temperature of the mixture was raised to 353 K and continuously stirred for an additional 22h. The pH of the solution was maintained at 8 throughout the 22h. The obtained precipitate was filtered using filter paper with a pore size of 0.2 μm, washed with deionized water and dried in ambient temperature for 5 days.

3.2.1 *Preparation of Zn-Cu-Ga LDH:*

Gallium nitrate hydrate is replaced in the place of Aluminum nitrate nonahydrate and the processor was repeated as same as mentioned for the above catalyst i.e., Zn Cu Al.

3.2.2 *Preparation of Zn-Cu-In LDH:*

Indium nitrate hydrate is replaced in the place of aluminum nitrate nonahydrate and the processor was repeated as same as mentioned for the above catalyst i.e., Zn Cu Al.

3.2.3 *Preparation of (Zn-Ni)-Cu Al LDH:*

Part of divalent i.e., Zn^{II} is replaced by Nickel.

A mixture of 20 ml solution of each Zinc nitrate hexahydrate of 0.25M+ Nickel nitrate hexahydrate of 0.125 M (total 0.375M), Copper nitrate trihydrate of 0.375M and Aluminum nitrate nonahydrate of 0.25M is dropped at the rate of 0.6ml/min into 100 ml of a 0.075 M Sodium carbonate solution in a flask with continuous mixing at a rate of 300 rpm. The pH was maintained at 8 by adding 1.0 M sodium hydroxide. After the complete addition, the mixture was continuously stirred at the same rate at room temperature for 2 h. Then the temperature of the mixture was raised to 353 K and continuously stirred for an additional 22h. The pH of the solution was maintained 8 throughout the 22h. The obtained precipitate was filtered using filter paper with a pore size of 0.2 μm, washed with deionized water and dried in ambient temperature for 5 days.

3.2.4 *Preparation of Zn-Cu (Al-In) LDH:*

Part of trivalent i.e., Al^{3+} is replaced by In^{3+}.

A mixture of 20ml solution of each Zinc nitrate hexahydrate of 0.375 M, Copper nitrate trihydrate of 0.375M and Aluminum nitrate nonahydrate of 0.17M + Indium nitrate hexahydrate of 0.08M (total= 0.25M) is dropped at the rate of 0.6ml/min into 100 ml of a 0.075 M Sodium carbonate solution in a flask with continuous mixing at a rate of 300 rpm. The pH was maintained at 8 by adding 1.0 M sodium hydroxide. After the complete addition, the mixture was continuously stirred at the same rate at room temperature for 2 h. Then the temperature of the mixture was raised to 353 K and continuously stirred for an

additional 22h. The pH of the solution was maintained at **8** throughout the 22h. The obtained precipitate was filtered using filter paper with a pore size of 0.2 μm, washed with deionized water and dried in ambient temperature for 5 days.

3.2.5 *Preparation of Zn-Cu (Al-Fe) LDH:*

Partition of trivalent ion i.e., Al^{3+} is replaced by Fe^{3+}

A mixture of 20ml solution of each Zinc nitrate hexahydrate of 0.375 M, Copper nitrate trihydrate of 0.375M and Aluminum nitrate nonahydrate of 0.05M + Iron nitrate hexahydrate of 0.20M (total= 0.25M) is dropped at the rate of 0.6ml/min into 100 ml of a 0.075 M Sodium carbonate solution in a flask with continuous mixing at a rate of 300 rpm. The pH was maintained at 8 by adding 1.0 M sodium hydroxide. After the complete addition, the mixture was continuously stirred at the same rate at room temperature for 2 h. Then the temperature of the mixture was raised to 353 K and continuously stirred for an additional 22h. The pH of the solution was maintained **8** throughout the 22h. The obtained precipitate was filtered using filter paper with a pore size of 0.2 μm, washed with deionized water and dried in ambient temperature for 5 days.

List of catalysts Prepared:

A. $[Zn_{1.5}Cu_{1.5}Al(OH)_8]_2^+ (CO_3)^{2-}$
B. $[Zn_{1.5}Cu_{1.5}Al(OH)_8]_2^+ (CO_3)^{2-}$
C. $[Zn_{1.5}Cu_{1.5}Al(OH)_8]_2^+ (CO_3)^{2-}$
D. $[Zn_{1.5}Cu_{1.5}In_{0.3}Al_{0.7}(OH)_8]_2^+ (CO_3)^{2-}$
E. $[Zn_{1.5}Cu_{1.5}Fe_{0.2}Al_{0.8}(OH)_8]_2^+ (CO_3)^{2-}$
F. $[Zn_{1.0}Ni_{0.5}Cu_{1.5}Al(OH)_8]_2^+ (CO_3)^{2-}$

3.2.6 *Preparation of CuO(3 %) loaded TiO_2 (P25) catalyst*

CuO(3 %) loaded TiO2 (P25) catalyst was prepared by impregnating copper nitrate solution on P25 catalyst . Appropriate amount of P25 and copper nitrate solution was taken together and sonicated for 1 h and then stirred for 4 hrs at 95°C. It was then dried at 150°C

for 2hrs at a ramp rate of 3°C/min .The dried sample was then calcined at 500°C for 0.5 h at the ramp rate of 5°C/min to obtain CuO(3 %) loaded TiO_2 (Slamet *et al*, 2005).

3.2.7 *Preparation of Ag(7 %) loaded TiO2 (P25) catalyst*

Ag(7%) loaded TiO_2 (P25) catalyst was prepared by impregnating Silver nitrate solution on P25 catalyst . Appropriate amount of P25 and silver nitrate solution was taken together and stirred well and then allow to rest for 24 hrs at RT. It was then dried in an oven at 100°C for 12hrs.The dried sample was then calcined at 400°C for 6h at the ramp rate of 5°C/min to obtain Ag(7 %) loaded TiO2 (*Sahoo et al., 2005*).

3.3 TECHNIQUES FOR CHARACTERIZATION OF CATALYSTS

3.3.1 *X-ray diffraction studies*

The crystal phase of the catalyst was analyzed by Rigaku X-ray diffractometer using CuKα radiation (λ=1.54056 A) in the scan range of 2θ = 5-90° at a speed of 3°/min.. The crystallite size of the catalyst samples were calculated by the Scherrer's formula (Patterson, 1939).

$$t = \frac{K * \lambda}{\beta * \cos \theta}$$

Where t = crystallite size

K = constant dependent on crystallite shape (0.9)

λ = X-ray wavelength (1.54056 A)

β = FWHM (full width at half maximum)

θ = Bragg's angle

The phase composition of TiO_2 was analyzed using the relative peak intensity of anatase and rutile (Spurr and Myers,1957).

$$F_A = \frac{1}{1 + 1.26(I_R / I_A)}$$

3.3.2 *Diffuse reflectance UV-Visible spectroscopic studies (DRS)*

Diffuse reflectance UV-Visible absorption spectra of the catalysts were recorded using a Thermo Scientific Evolution 600 spectrophotometer equipped with a Praying mantis diffuse reflectance accessory.

3.3.3 *Surface area measurements*

Surface area and pore volume of the catalysts were measured using Micromeritics ASAP 2020. Degassing of the sample was done at 373 K for 2 h and at 423 K for 3 h. For adsorption experiments, pure nitrogen was used at liquid nitrogen temperature.

3.3.4 *Scanning electron microscopic (SEM) analysis*

Scanning electron micrographs were recorded using FEI, Quanta 200. The samples in the powder form were taken on the carbon tape and mounted on the SEM sample holder.

3.3.5 *FT- IR Spectroscopic analysis*

FT-IR spectrum of prepared power catalyst were recorded using Spectrum one: FT-IR spectrometer, with the scan range MIR 450-4000cm^{-1} and resolution 1.0cm^{-1} .

3.4 CO_2 photoreduction studies

Reaction studies were conducted in batch mode, in liquid and vapor pahse.

a. Liquid phase reactor

The schematic representation of the photo catalytic reactor set up is shown in the Scheme 2. The Photo catalytic reduction was carried out in a glass reactor with a window through which CO_2 medium was irradiated. A quartz plate of dimension 7cm*7cm was fitted into the window. Catalyst (0.4 g) and 400 ml of 1M NaOH was added to the reactor. After bubbling CO_2 for 30 min, the reaction medium was irradiated. The reactor was tightly

closed during the reaction. The solution in the reactor was continuously stirred by a magnetic stirrer during irradiation by 250 W Hg lamp. Reactions were carried out using Zn-Cu-Al LDH in the liquid phase reaction.

• Reactor volume – 620 ml

• Reaction medium - 400 ml of 0.2 N NaOH .

• Catalyst loaded - 0.4 g .

• CO2 was bubbled for 30 min.

• Reaction medium was irradiated through a 5 cm diameter quartz window.

• Hg lamp with 77 W power was used.

b. Analysis of products

• The products were analyzed using Clarus 500 Perkin Elmer Gas chromatography using Poroplot Q, 30 m and the detector is FID.

Injector Temperature : 250°C

Column Temperature : 150°C isothermal, Hold – 20 min

Detector Temperature : 250°C

Carrier Gas : Nitrogen, 1.5 ml/min.

• Methane (10 % in N_2), Ethane (5% in N_2) methanol, acetone, acetaldehyde, ethanol were injected and their retention time were noted. All the compounds were detected in gas phase. Therefore , all the liquid compound were taken, purged with N_2 and then the gas phase which now contains both the compound and N_2 was injected into the GC for calibration. The amount injected was 0.3 ml.

• During the reaction, gas samples (0.3 ml) were withdrawn every one hour from the reactor and injected into the GC.

Schematic Representation of Photo Catalytic Reactor for Liquid Phase:

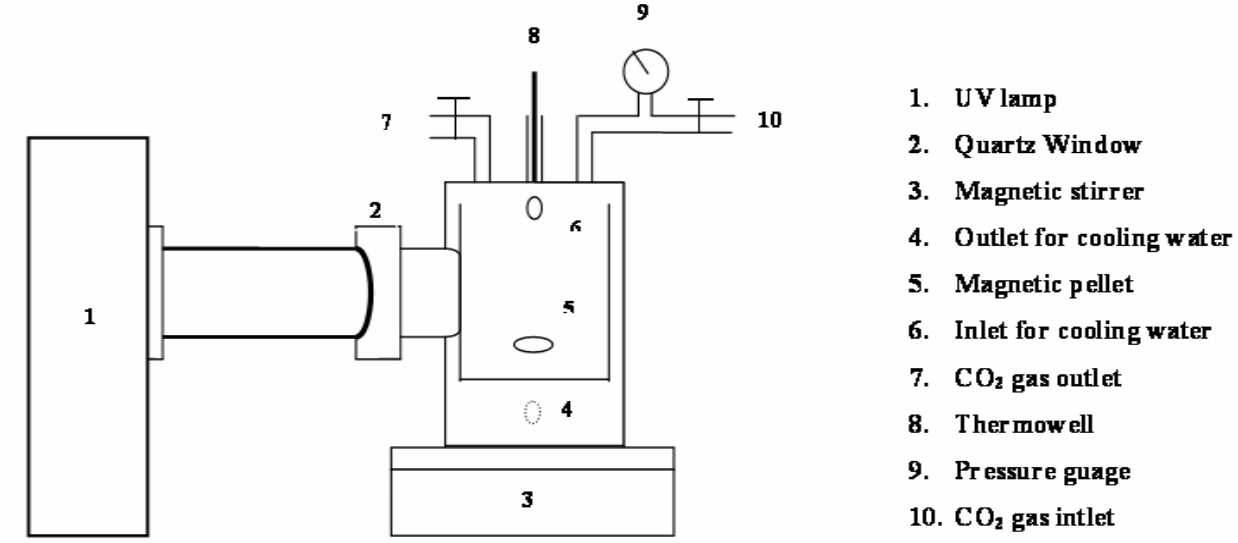

Scheme 2: Set up of photo catalytic reactor for liquid phase.

Blank experiments were conducted to ensure that the product formed was due to the photoreduction of CO_2. The blank tests consist of a UV-illuminated without the catalyst and a reaction in the dark with the catalyst.

The intensity of the lamp was measured by lux meter and it was found to be 77000 lux which was then converted into Watts with the help of the spectral distribution of the lamp. Using fibre optics spectra analyzer (Ocean optics), the spectral distribution of Hg lamp was found.

The illumination constitutes 37.3 % of ultra violet radiation (23.8% for λ=335 nm and 14.5% for λ=365 nm) and the remaining visible region.

c.Reaction in vapor phase

Schematic Representation of Photo Catalytic Reactor for Vapor Phase:

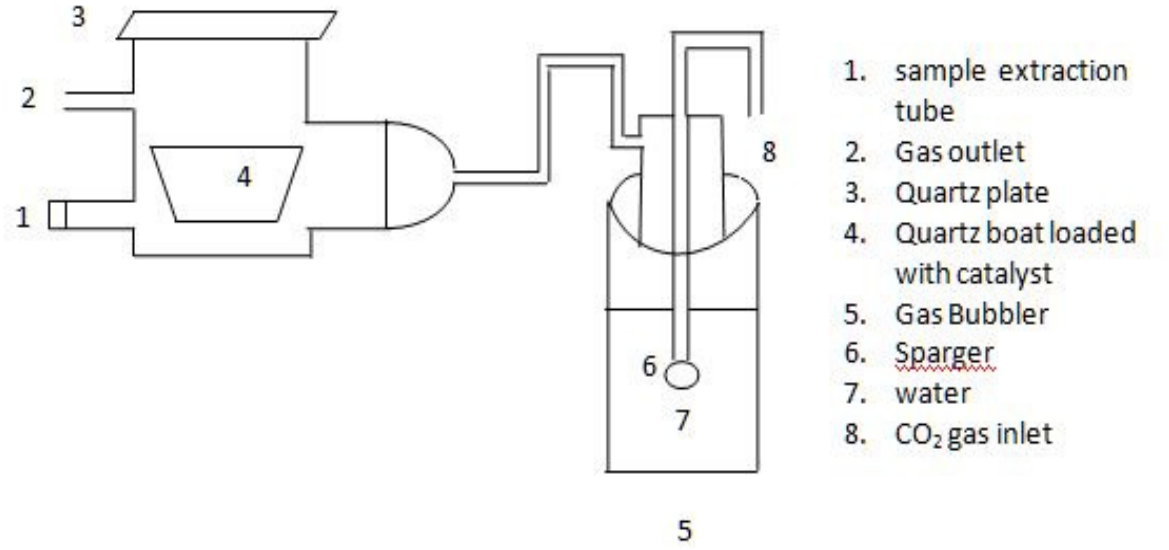

Scheme 3: Set up of Photo catalytic reactor for vapor phase.

The Photo catalytic reduction was carried out in a glass reactor with a quratz window through which CO_2 medium was irradiated (8). A quartz plate of dimension 7cm*7cm was fitted as the window. Catalyst (0.4g, 0.2g & 0.1g) was kept inside the reactor on the rough surface of a glass plate of size 7*4cm. After purging and filling the reactor with CO_2 gas saturated with water vapor for 30 min, the reactor was tightly closed during the reaction. Vapor phase reactions were carried out on all the prepared catalysts.

d. Design of Solar Reactor for Reduction of Carbon Dioxide for both liquid & Gas phase:

A solar Photo Chemical reactor is a device to test the activity of various catalysts for reduction of carbon dioxide and water under sunlight. The reactor consists of a rectangular white acrylate sheet (3mm thickness & 20*20cm size) covered with a layer of the photoactive material.

Set up:

A schematic representation of solar reactor is shown in Scheme 4. Solar reactor is made up of stainless steel of rectangular base plate (30*25cm) thickness 3mm, having the gas inlet, liquid sampling point and outlet at the bottom left and at the right top of the reactor of 2cm length and 1cm dia. The acrylate tube of 1.5cm dia with 3mm pitch distance between two holes on the tube is maintained such that the carbon dioxide is passed through it into the reactor for better dispersion of the entering gas. The reactor consists of a white acrylate sheet which is of same size as the base plate and is separated by a rubber gasket of 2mm thickness which is tightened to the base plate using screws without any leakage and is fixed 45^0 inclination from the ground surface towards the sunlight. The thermo well is fixed at the top left side of the reactor so that the temperature is measured using thermometer. The acrylate sheet of 20*20cm is taken and the surface of the sheet is roughen using the 279 medium size emery paper such that the prepared catalyst is coated on the plate using spray.

The catalyst coated acrylate sheet is fixed inside the reactor on the base plate and on the top of it, acrylate sheet is fixed using the rubber gaskets and is tightened using screws for leak proof. The carbon dioxide saturated with water vapor is passed through the stop cock through the acrylate tube into the reactor for 30min and then the stop cocks are closed at the both gas inlet and gas outlet points.

Now, the reactor is kept under sunlight and for every one hour the sample is collected from the sampling point in the top of reactor and is injected into the gas chromatography. Thus this process is repeated for 7 to 8hrs. This is for gas phase reaction.

Important NOTE: The major Advantage of this solar reactor is, it can be used for both Liquid as well as vapor phase reaction to convert carbon dioxide into useful fuels as methane, ethane, acetaldehyde etc.,

Schematic Representation of Photo Catalytic Reactor for Direct Sun Light for both liquid & Vapor phase:

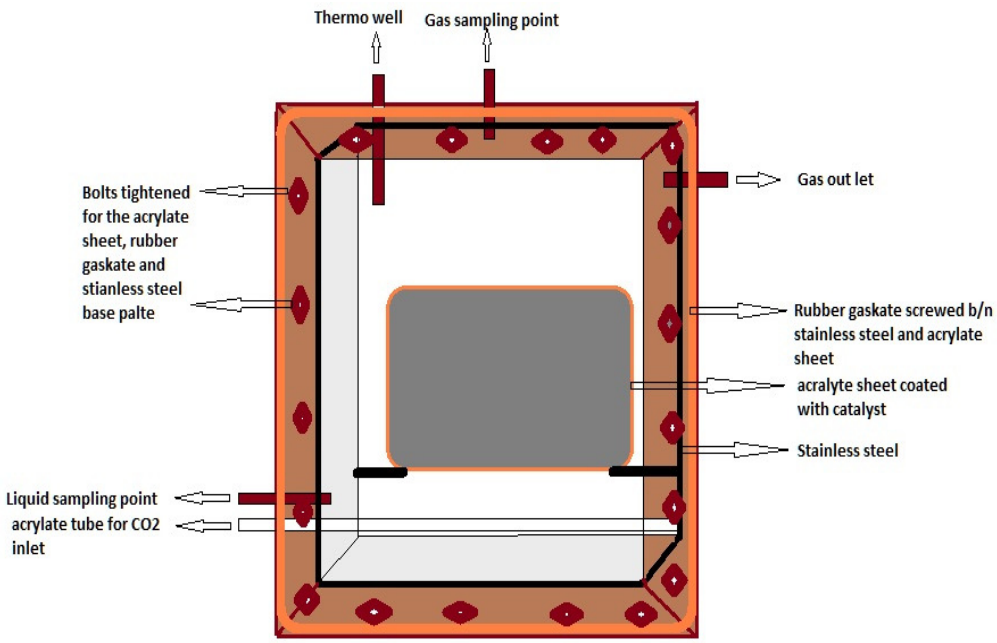

Scheme 4: Set up of solar reactor for both liquid & Vapor phase.

CHAPTER 4
RESULTS & DISCUSSIONS

4.1 Synthesis and characterization of LDH catalysts

4.1.1Textural properties

Three ternary and three quaternary LDH catalysts were synthesized as per the procedures described in Chapter 3. Textural characteristics of the three ternary LDH catalysts are tabulated in Table 1.Surface area values of prepared catalysts are comparable with those reported in literature (*Ahmed et.al*., 2011). Pore volume and pore-size data for these catalysts have not been reported in literature.

TABLE 4: TEXTURAL PROPERTIES OF HYDROTALCITES

Sample	Surface area m^2/g	Pore vol. cm^3/g	Pore dia. Å
Zn Cu Al	25.6	0.189	305.0
Zn Cu Ga	47.1	0.186	127.9
Zn Cu In	72.8	0.394	202.6

4.1.2 Phase analysis by XRD

XRD patterns for all six LDH catalysts are presented in Figs.4.1.2 (a) - 4.1.2 (f) along with the diffraction profile recorded for the measurement of crystallite size by line broadening. XRD data for the sample $[Zn_{1.5}Cu_{1.5}Al(OH)_8]_2^+ (CO_3)^{2-}$ (Fig.4.1.2 (a) [Zn-Cu-Al]) shows all major d-lines due to hydrotalcite phase, at 2θ values, 11.7, 23.5, 34.6, 37.3,39.2,43.9,46.7, 52.9, 56.3, 60.2 and 61.5 & 65.5 (*Ahmed et al., 2011*).

On complete substitution of Al by Ga, the 2θ angles of plane –to-plane diffraction peaks (0 0 3), (0 0 6) and (0 0 9) perpendicular to the cationic layers remain the same ,but other peaks are significantly shifted towards smaller angles, reflecting the larger ionic radius of Ga^{III} compared to Al^{III}. For example, 2θ for (110) plane is 60.2° for Al which changes to 59.5° for Ga-containing LDHs (Fig 4.1.2 (b) [Zn-Cu-Ga]). Some minor peaks at 2θ= 27.9,

30.3, 35.7, 57.3 and 62.9 degrees were also observed, which were possibly due to some impurity (*Ahmed et al., 2011*).

XRD data for In based hydrotalcite of the expected composition $[Zn_{1.5}Cu_{1.5}In(OH)_8]_2^+$ $(CO_3)^{2-}$, (Zn-Cu-In), has not been reported. Though d-lines due to typical hydrotalcite phase are observed, their intensities are less and a major peak due to $In(OH)_3$ is observed (Fig 4.1.2 (c)). Since In^{3+} size is larger than Al^{3+} (0.081. Vs 0.056 nm) complete substitution of Al^{3+} by In^{3+} may not be possible resulting in the separation of $In(OH)_3$..

In view of this, partial substitution of Al^{3+} by In^{3+} corresponding to LDH of the composition $Zn_{1.5}Cu_{1.5}In_{0.3}Al_{0.7}$ $(OH)_8(CO_3)^{2-}$ has been attempted. XRD pattern for this phase is presented

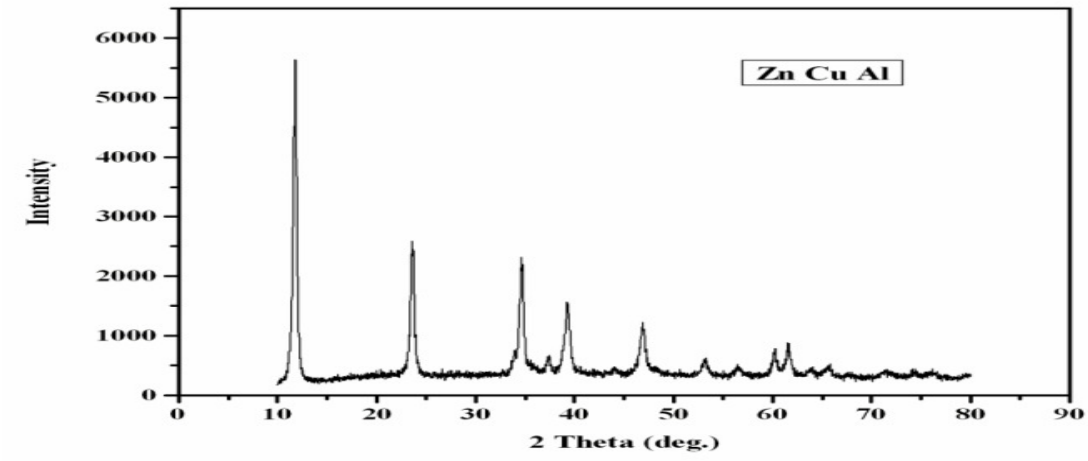

Fig 4.1.2 (a): XRD pattern for Zn Cu Al

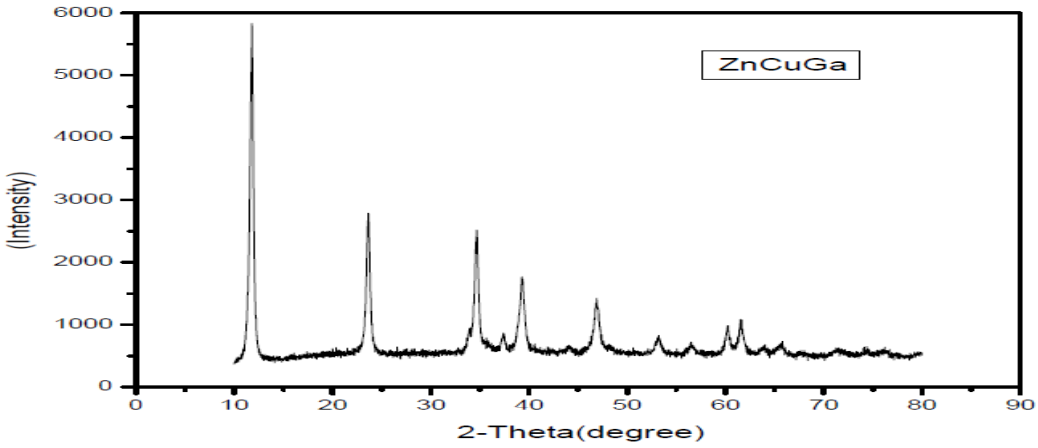

Fig 4.1.2 (b): XRD pattern for Zn Cu Ga

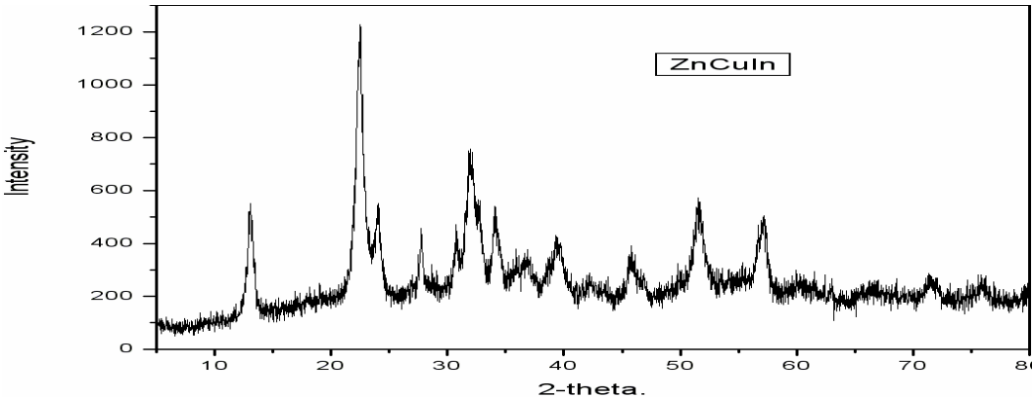

Fig 4.1.2 (c): XRD pattern for Zn Cu In

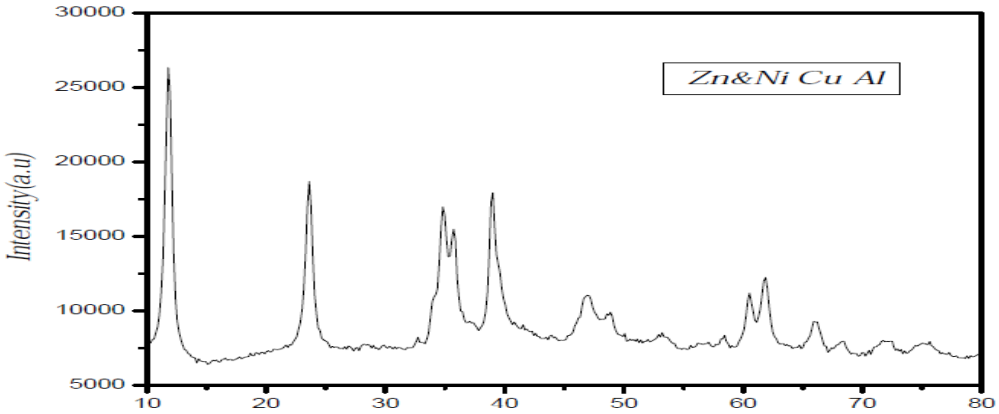

Fig 4.1.2 (d): XRD pattern for Zn&Ni Cu Al.

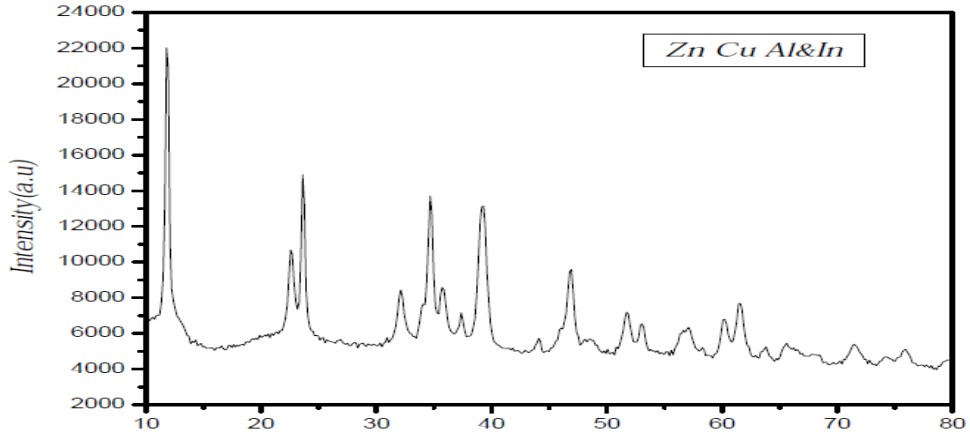

Fig 4.1.2 (e): XRD pattern for Zn Cu Al&In.

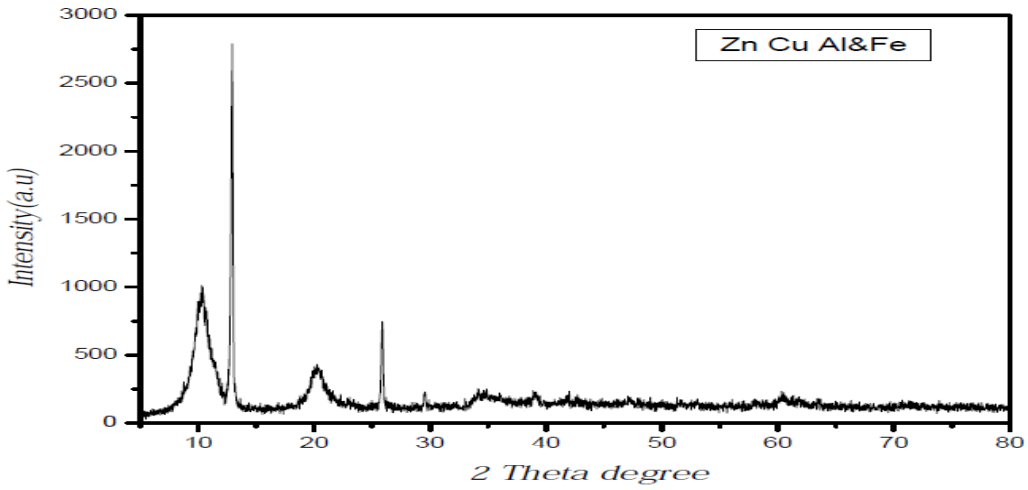

Fig 4.1.2 (f): XRD pattern for Zn Cu Al&Fe.

in Fig 4.1.2 (e). It is observed that hydrotalcite appears as the major phase, along with $In(OH)_3$ as the minor phase. It is likely that pure hydrotalcite phase could be formed at still lower levels of In ion (~ 0.2 atomic fraction or less) incorporation in the place of Al ion. Further work is needed to establish this point.

However, LDH catalysts with partial substitution of divalent Zn by Ni, corresponding to the composition, $[Zn_{1.0}Ni_{0.5}Cu_{1.5}Al(OH)_8]_2^+$ $(CO_3)^{2-}$ ([Zn-Ni]-Cu-Al) results in pure hydrotalcite phase as observed in the XRD pattern (Fig.4) with the d-lines at $2\theta=34°$ showing a doublet.

Partial substitution of Al^{3+} by another trivalent ion, Fe^{3+}, as (Zn-Cu-[Al-Fe]) with the composition $[Zn_{1.5}Cu_{1.5}Fe_{0.2}Al_{0.8}(OH)_8]_2^+$ $(CO_3)^{2-}$ results in a hydrotalcite phase but with amorphous character, as indicated by highly diffused peaks (Fig.4.1.2 (f)).

Crystallite size values for all six samples, as measured by X-ray line broadening analysis, are in the range 12 –46 nm, indicating that the samples are nanosized (Table 5).Though all samples were prepared by adopting same procedure, ([Zn-Ni]-Cu-Al) phase displayed minimum size. It is well known that crystallite size of the catalysts influence their photocatalytic activity.

4.1.3 FT-IR spectra

FT-IR spectra for all six LDH catalyst samples recorded in the range 4000-500 cm^{-1} are displayed in Figs 4.1.3 (a) - (f). Based on the IR spectra data for different hydrotalcite phases published in literature (*Kannan et al., 2005*), the data for the samples prepared in this work have been analysed. The spectra for all the six samples are more or less similar, with slight variations in the intensity of absorption bands. Range of absorption bands corresponding to various functional groups observed in the LDH samples prepared in this work are given below:

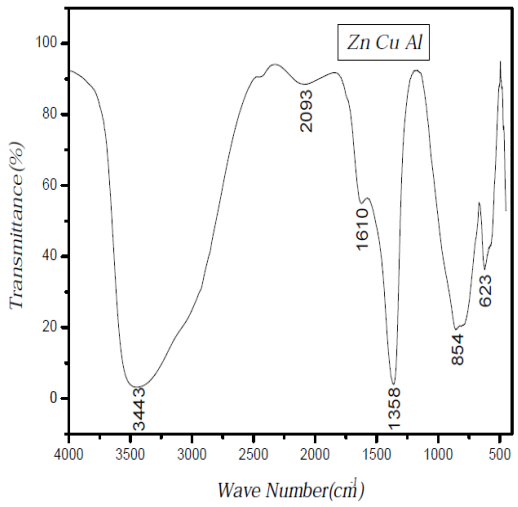

Fig 4.1.3 (a): IR Spectra for Zn Cu Al.

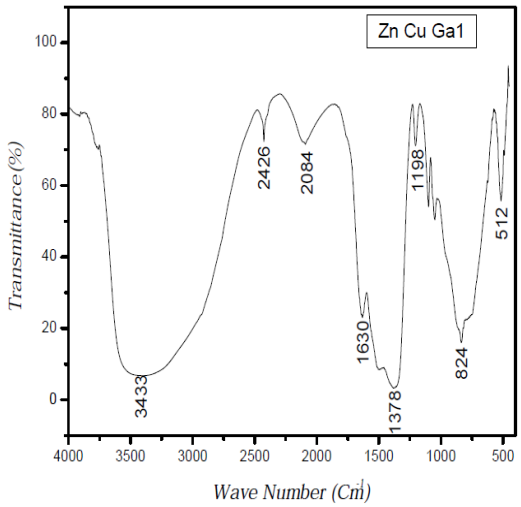

Fig (b): IR spectra for Zn Cu Ga.

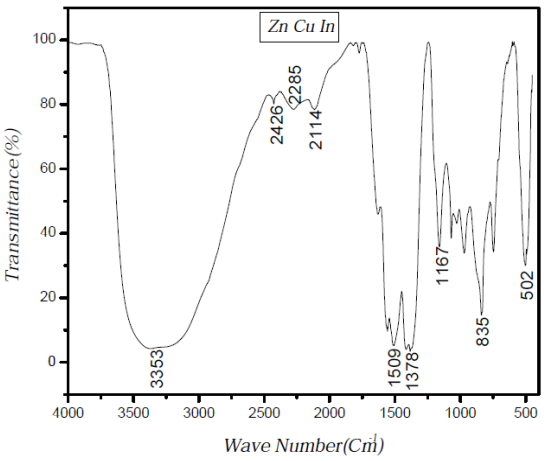

Fig (c): IR spectra for Zn Cu In.

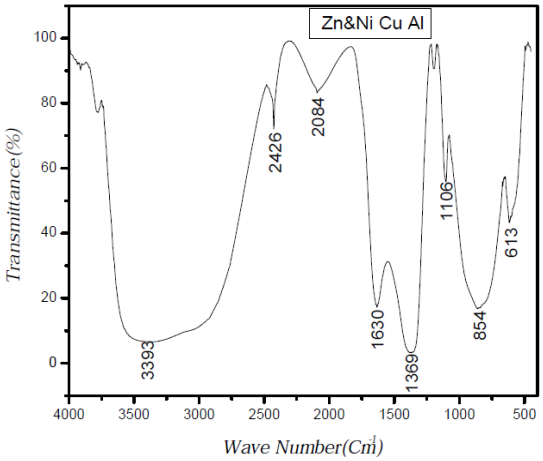

Fig (d): IR spectra for Zn&Ni Cu Al.

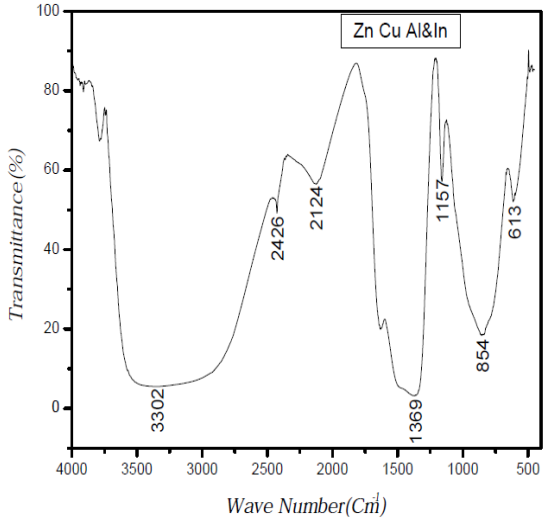

Fig (e): IR spectra for ZN Cu Al&In.

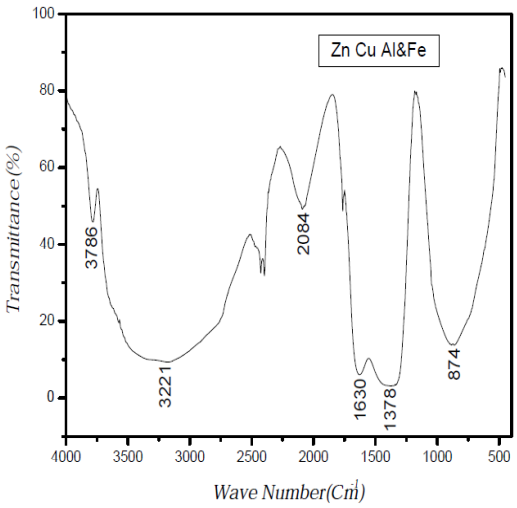

Fig (f): IR spectra for Zn Cu Al&Fe.

a) 3200-3500 cm^{-1} – Due to surface –OH groups both from brucite layer and water in inter layer space
b) 1610-1630 cm^{-1} – Attributed to deformation mode of water
c) 1360-1380 cm^{-1}- ν_3 asymmetric stretching of CO_2
d) 830-870 cm^{-1}- due to carbonate species
e) 500-700 cm^{-1}- Assigned to M-OH and M-O bonds.

Besides these major absorption bands several other bands in the ranges 2000-2400 cm^{-1}, and 1150-1170 cm^{-1} have been observed with all samples, though their significance is not known at present. Characteristic band of nitrate group expected at 1385 $cm^{-1}$is not observed with any of the samples, indicating that washing has effectively removed the nitrate species. Though all bands corresponding to hydrotalcite species have been observed, presence of some metal oxidic/hydroxyl groups cannot be ruled out as evidenced by the XRD data.

4.1.4 UV-Visible diffuse reflectance spectra

DR spectra for all the six LDH samples in the range 200-800 nm are shown in Fig 4.1.4 (a) – (f). Band gap values calculated by standard method are tabulated in Table.5 along with crystallite size data.

TABLE 5:

CRYSTALLITE SIZE & BAND GAP VALUES FOR HYDROTALCITES.

Sample	Crystallite Size(nm)	Band Gap(eV)
Zn Cu Al	20.4	4.1
Zn Cu Ga	25.4	3.5
Zn Cu In	21.2	3.1
Zn&Ni Cu Al	12.6	3.3
Zn Cu Al&In	25.7	3.2
Zn Cu Al&Fe	46.4	1.9

Partial or complete substitution of trivalent Al ion by Ga & In bring down the band gap value considerably from 4.1 eV to 3.5 -3.1 eV and to 1.9 eV by substitution with Fe. Partial substitution of Zn by Ni also lowers the band gap value to 3.3 eV. Thus substitution of trivalent Al or divalent Zn results in shifting of the absorption band edge towards visible

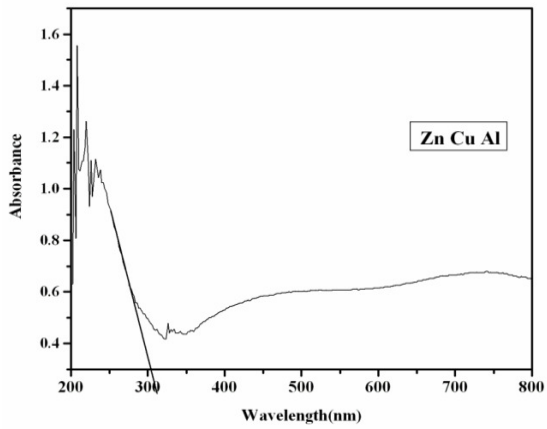

Fig 4.1.4 (a): UV spectra of Zn CuAl

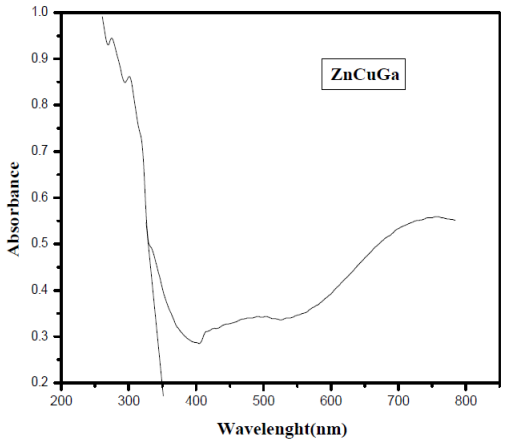

Fig (b): UV spectra of Zn Cu Ga.

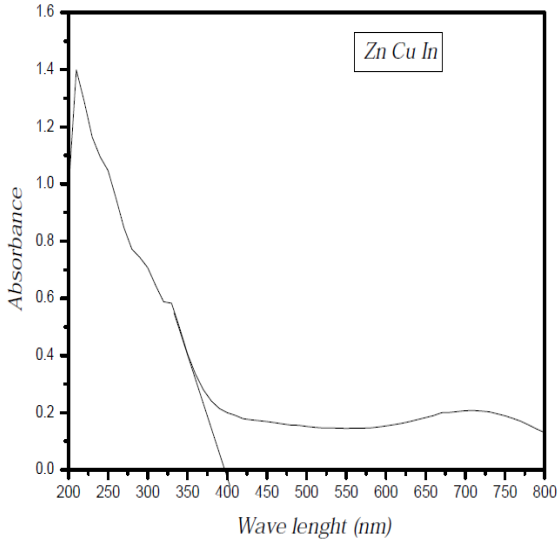

Fig (c): UV Spectra for Zn Cu In.

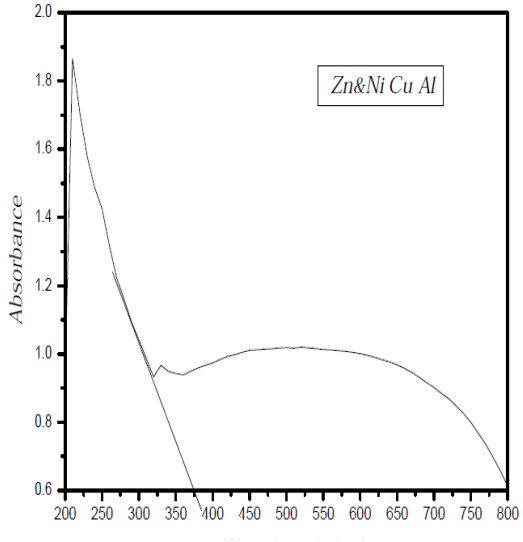

Fig (d): UV Spectra for Zn&Ni Cu Al.

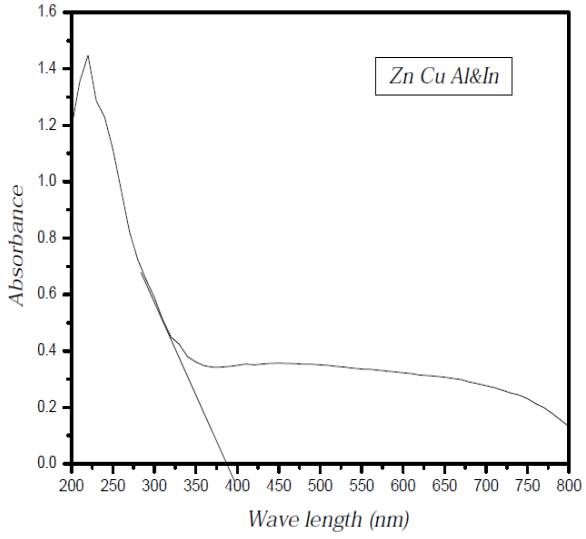

Fig (e): UV Spectra for Zn Cu Al&In.

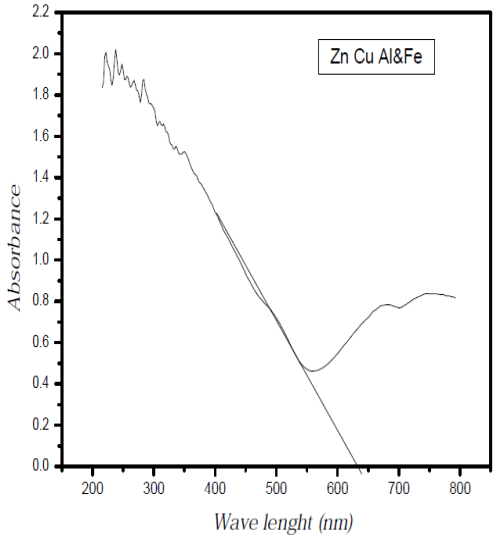

Fig (f): UV Spectra for Zn Cu Al&Fe.

range. Such changes in electronic energy levels of hydrotalcites would have direct bearing on the photocatalytic activity and the product profile during photocatalytic reduction of CO_2 with water. These aspects are discussed in the following sections.

4.1.5 Scanning electron microscopy & EDAX

SEM micro graphs of four LDH catalyst samples (Zn-Cu-Al), (Zn-Cu-Ga), (Zn-Cu-In) and (Zn-Cu-[Al-In]) at fixed magnification settings are shown in Figs 4.1.5 (a) - (d)

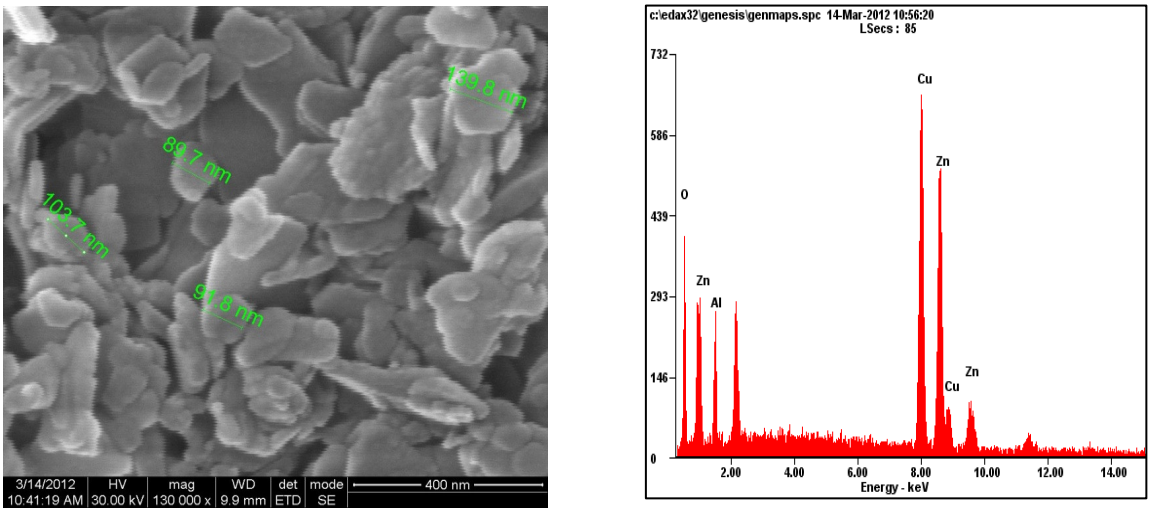

Fig 4.1.5 (a): SEM & EDAX for Zn Cu Al catalyst.

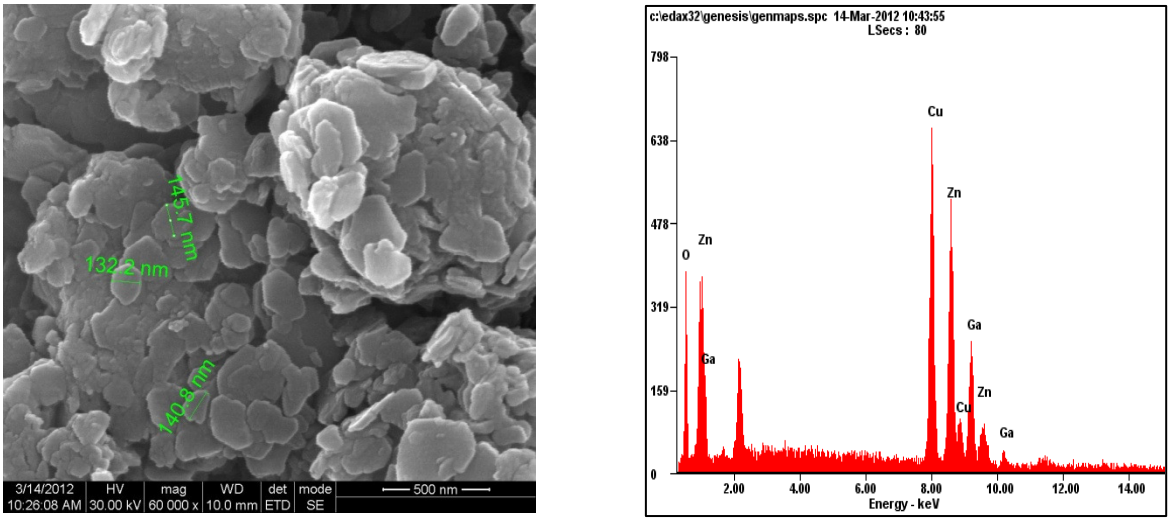

Fig (b): SEM & EDAX for Zn Cu Ga catalyst.

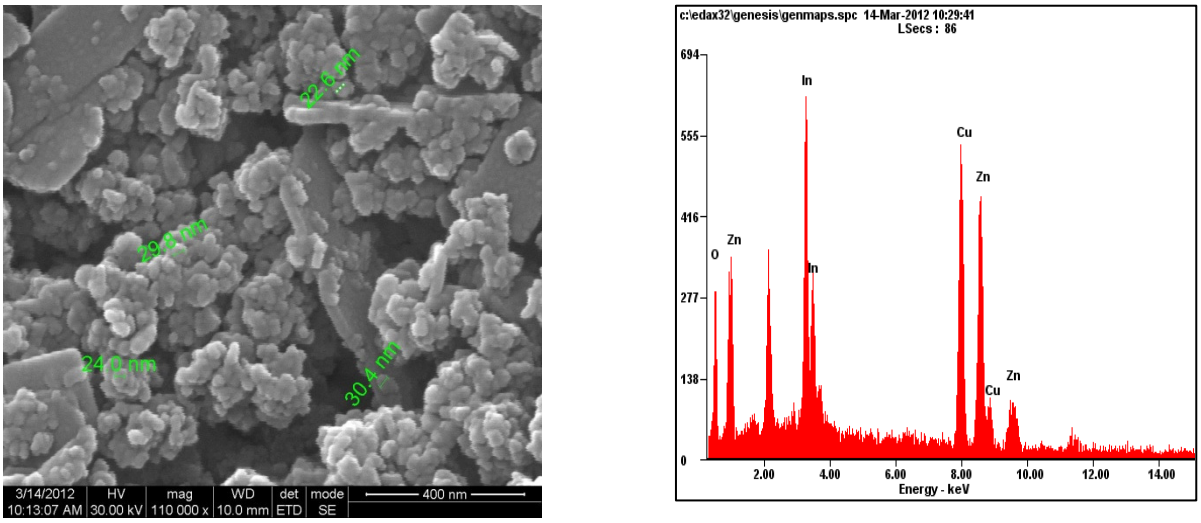

Fig (c): SEM & EDAX for Zn Cu In catalyst.

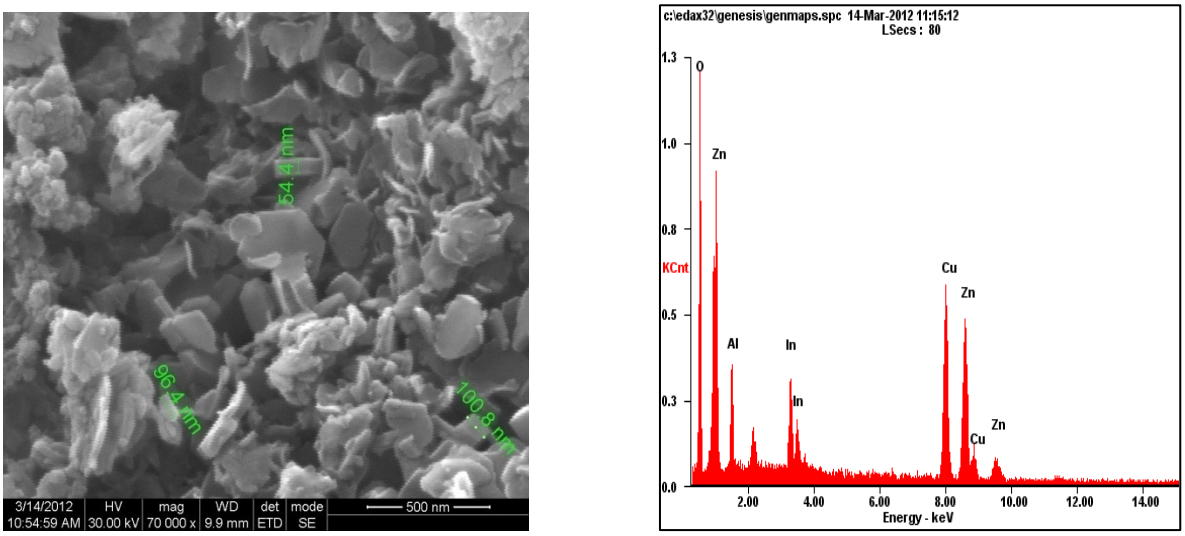

Fig (d): SEM & EDAX for Zn Cu Al&In catalyst.

All of them display flat flaky or plate like morphology, with particle size in the range 20-150 nm. *Ahmed et al., 2011* reported particles of size < 100 nm and observed that this morphology is characteristic of layered hydrotalcite structure. Larger flakes of different sizes observed are formed by coagulation and hence the variation in size.

4.2 Evaluation of LDH catalysts for photocatalytic reduction of CO_2 with water (PCR)

For evaluation of PCR, all LDH samples at dried stage, without any further heat treatment were used. Catalysts were evaluated in batch mode in two different phases,

a) in aqueous phase, wherein the catalyst is dispersed in 0.2 molar NaOH and saturated with CO_2 gas

b) in vapour phase, wherein CO_2 gas saturated with water vapour is in contact with the catalyst kept in quartz boat or etched glass plate.

In case a), water is present in excess compared to CO_2 and hence may generate more hydrogen by water splitting and accordingly the photocatalytic reduction of CO_2 may be deeper. Both gas phase and liquid phase samples are to be analysed for products.
In case b) CO_2 is in excess vis-à-vis water and hence CO_2 photoreduction could proceed to a limited extent. Analysis of gas phase samples would be required.

4.2.1 Evaluation of Zn-Cu-Al in aqueous & vapour phase

For the sake of comparison, the activity of the catalyst (0.4 g in each case) was evaluated in aqueous and vapor phase. While 0.4 g of catalyst was dispersed in aqueous solution of 0.2M NaOH for vapour phase reaction, 0.4g of catalyst was kept in a quartz boat and exposed to radiation in presence of CO_2 gas saturated with water vapour. In the case of aqueous phase evaluation, products in measurable quantities could be detected only in vapour phase. Methane, ethane, methanol, ethanol and acetaldehyde were the products identified in both cases. Amounts of methane and ethane formed were too less for reliable quantitative estimation.

Quantities of methanol, ethanol and acetaldehyde formed in aqueous and vapor phase reactions are displayed in Fig, 26 to 30. Methanol and ethanol formation decrease with respect to time, possibly due to deactivation of the catalyst.

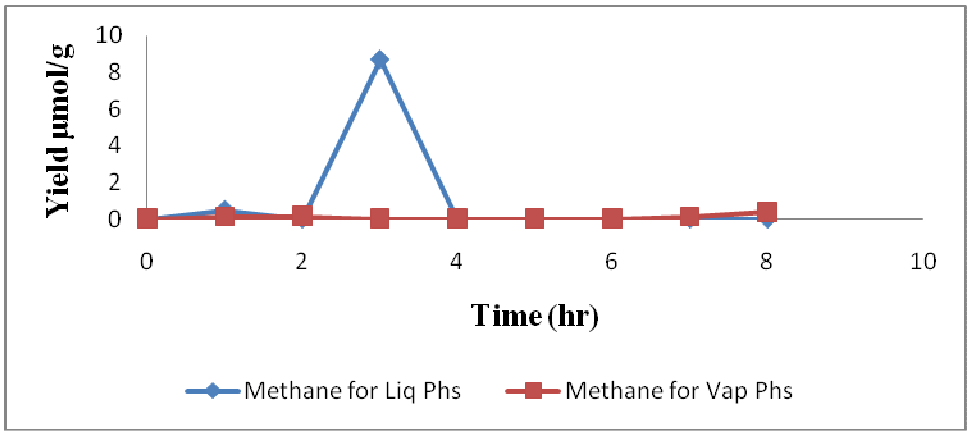

Fig 26: Methane formed for both Liquid & vapor Phase.

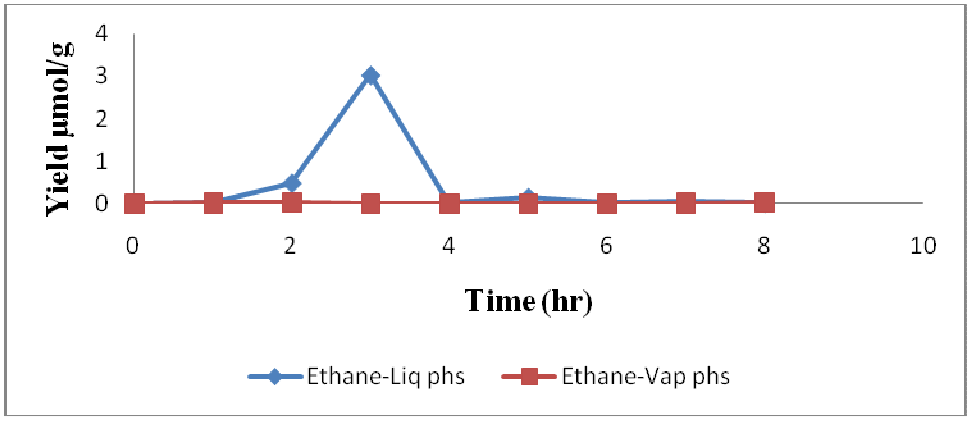

Fig 27: Ethane formed for both Liquid & vapor phase.

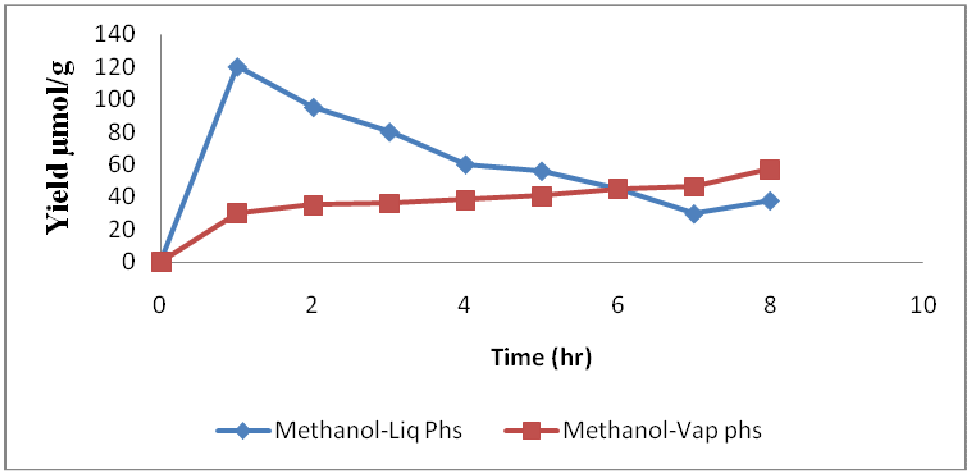

Fig 28: Methanol formed for both liquid & Vapor phase.

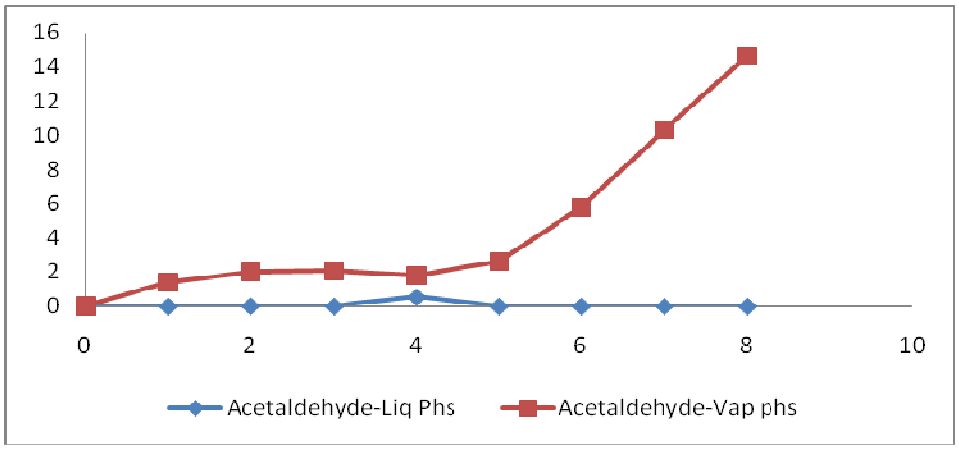

Fig 29: Acetaledhyde formed for both Liquid & Vapor phase.

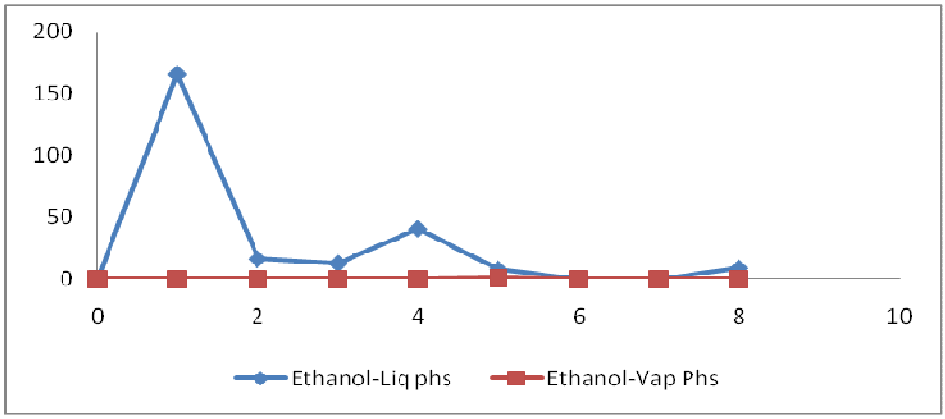

Fig 30: Ethanol formed for both liquid & Vapor phase.

There is noticeable change in the product profile in both phases. Methanol and ethanol with very little amount of acetaldehyde is formed in aqueous phase, while only methanol and acetaldehyde are observed in vapour phase. Ethanol is not observed in vapour phase. Besides, the total amount of hydrocarbons formed in aqueous phase is higher than that in vapour phase.

This difference in the reactivity and the product profile is due to the availability of the reducing agent, hydrogen. In aqueous phase availability of water in excess ensures higher hydrogen production by water splitting and hence reduction of CO_2 could proceed upto ethanol stage. In the vapour phase CO_2 is in excess and availability of hydrogen is less and

hence reduction stops at acetaldehyde stage. For the same reason, overall conversion in aqueous phase is higher.

4.2.2 Evaluation of all catalysts in vapour phase

Ahmed et al., 2011 have studied the photoreduction of CO_2 on hydrotalcites with external hydrogen in vapour phase in a closed circulating reactor. In order to get data comparable with those of *Ahmed et al., 2011,* reactions were studied in vapour phase.

In section 3.2.1 vapour phase studies on Zn-Cu-Al catalysts were carried out with 0.4 g of catalyst. Since the catalyst was kept as a thick layer in a quartz boat, it is possible that only the top layer was energised with the radiation. To circumvent this limitation in exposure of the entire catalyst mass to the radiation, 0.1 g of the catalyst was spread as a thin layer within the rectangular etched surface of a glass plate. CO_2 gas saturated with water vapour by bubbling through a water column was used as reactant. The formation of different products with respect to time for five different catalysts, namely, Zn-Cu-Ga, Zn-Cu-In, Zn-Cu-[Al-Fe], Zn-Cu-[Al-In] and [Zn-Ni]-Cu-Al are given in Figs 31-34. Reduction of CO_2 to methane and ethane is extremely low, but conversion to methanol and acetaldehyde are substantial. As observed with vapour phase reduction on Zn-Cu-Al, in the case of these five catalysts too, ethanol is not formed. This indicates that in the absence of sufficient water for hydrogen generation, the degree of CO_2 reduction is restricted to acetaldehyde level. It has been reported by *Anpo et al., 1997* that CO_2: water mole ratio of 1:5 is optimum for methane formation.

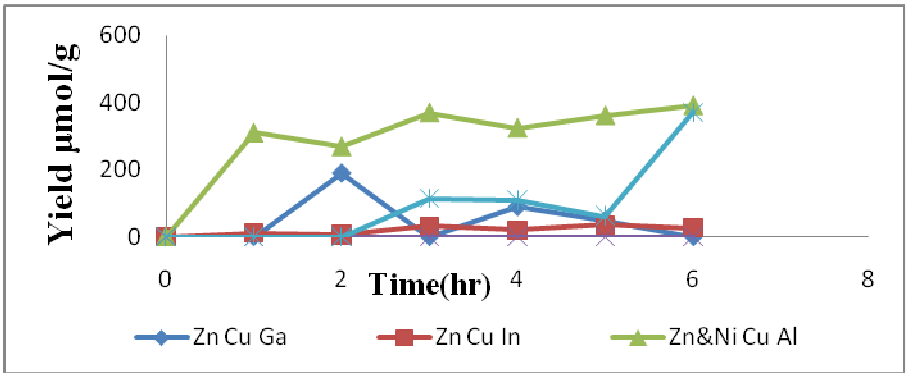

Fig 31: Methanol formed for ALL catalysts.

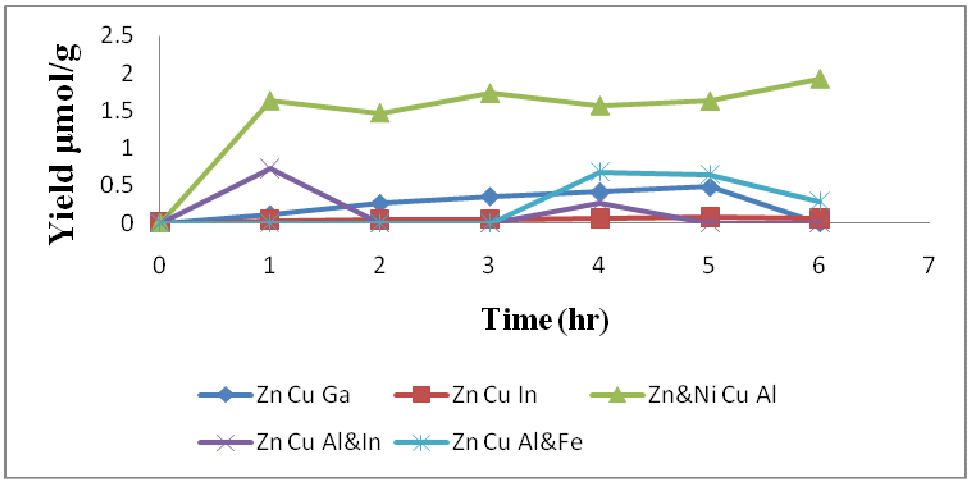

Fig 32: Methane values for ALL catalysts.

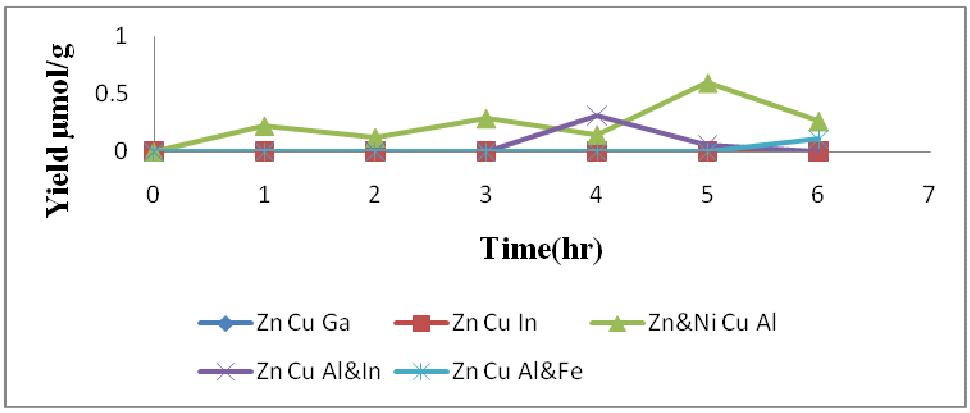

Fig 33: Ethane formed for ALL catalysts.

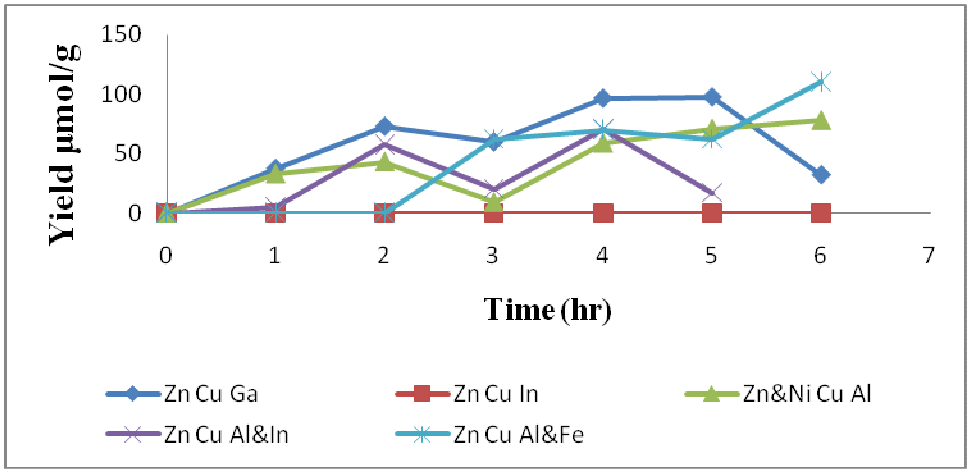

Fig 34: Acetaldehyde formed for ALL catalysts.

Maximum conversion to methane, ethane and methanol (~350 micro moles/g) is observed on [Zn-Ni]-Cu-Al catalyst followed by Zn-Cu-Ga. [Zn-Ni]-Cu-Al also displays stable activity for more than 6 hrs. Both Zn-Cu-[Al-Fe] and Zn-Cu-[Al-In] catalyst systems display good activity after some induction period. Based on the product patterns observed for the six catalysts, the order of activity for methanol formation increases in the following order:

Zn-Cu--In] < Zn-Cu-[Al-In] < Zn-Cu-[Al-Fe] < Zn-Cu-Al< Zn-Cu-Ga < [Zn-Ni] -Cu-Al

The following are the significant outcome of the investigation at this stage:

- Substitution of the divalent Zn by Ni brings about substantial increase in the overall activity for CO_2 photoreduction.
- Substantial changes in the band gap values observed for various hydrotalcite samples (Table.2) could be one of the reasons for the observed differences in the activity. Shifting of light absorption edge towards visible range would increase the activity with visible light.
- In the case of [Zn-Ni] –Cu-Al very small particle size could be an additional factor for the observed increase in activity.
- For many photocatalysts based on perovskite/pyrochlore structure, NiO is identified as highly efficient co-catalyst.
- In this context, it is worth exploring the whole range of compositions from Zn-Cu-Al to Ni-Cu-Al and also the incorporation of Ni in Zn-Cu-Ga system.
- Though the band gap for Zn-Cu-[Al-Fe] is less its amorphous nature and larger crystallite size may adversely affect the activity
- In the case of In based hydrotalcites, presence of free $In(OH)_3$ as additional phase as observed in XRD patterns could affect the performance.

4.2.3 Evaluation of photocatalysts using solar reactor

A solar reactor as described in Chapter 3. was used to study the PCR of CO_2 using direct sunlight for activation. Three different catalysts, P-25, 7% Ag/P-25 and 3% CuO/P-25, were evaluated in vapour phase. Aqueous slurry of the catalysts were coated as thin layer

on roughened (by using emery paper) acrylate sheet. The reactor was aligned to the direction of sun's radiation, which was tracked continuously for about 5-6 hours, by periodical realignment of the reactor so as to expose the reactor to the sun. Product patterns observed for the catalysts are displayed in Figs 35 to 37. While all the three major products methanol, ethanol and acetaldehyde are

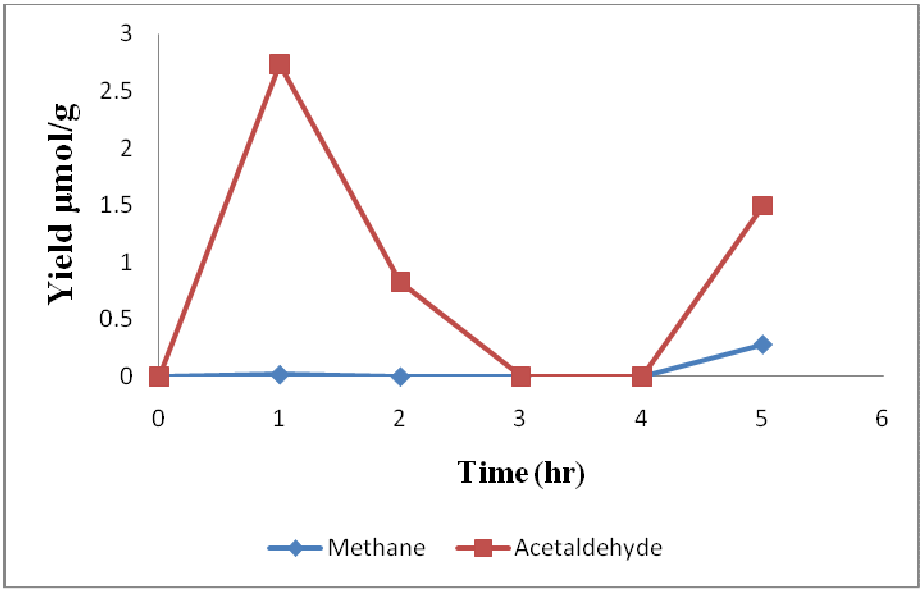

Fig 35: P-25 formed for Solar reactor.

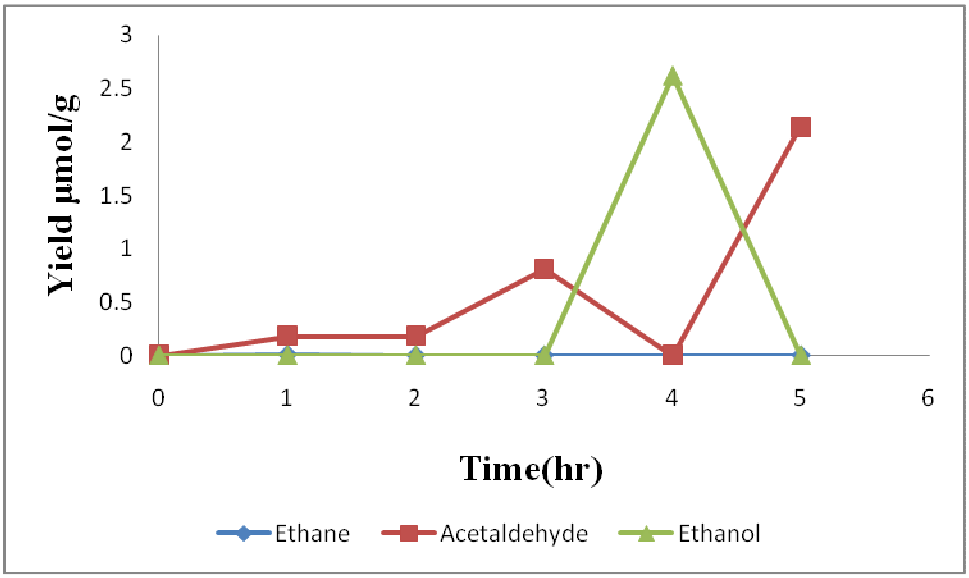

Fig 36: CuO/P-25 formed for Solar reactor.

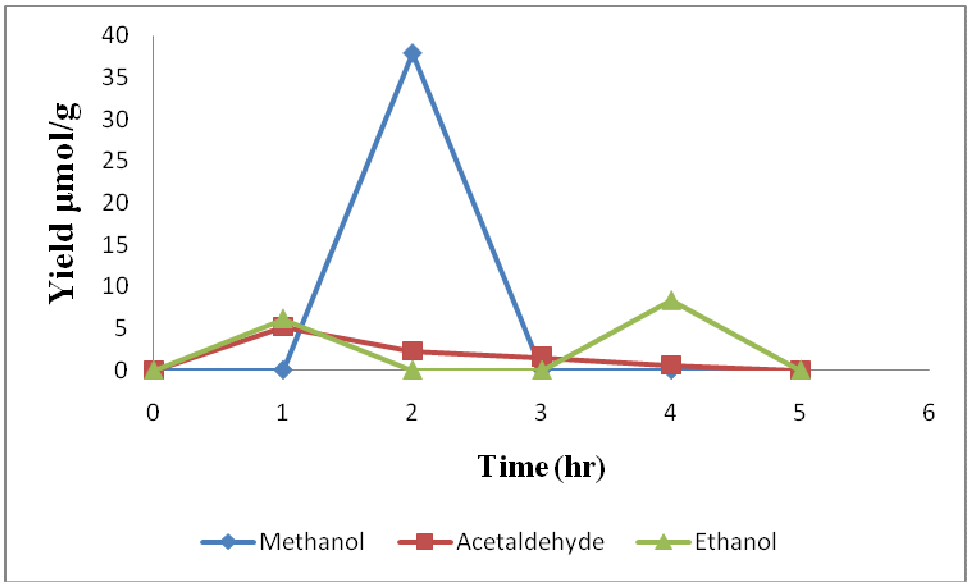

Fig 37: Ag/P-25 formed for Solar reactor.

observed with all catalysts, maximum conversion is realized with P-25. After about 3-4 hours, the activity of the catalyst is reduced drastically.

Increasing the partial pressure of water and conducting experiments in aqueous phase would increase the CO_2 reduction.

4.2.4. CO_2 photoreduction on hydrotalcite catalysts

There has been only one reference (*Ahmed et al., 2011*) on photocatalytic reduction of CO_2 on hydrotalcites. Direct comparison of the reported data with the current investigation is not straightforward due to the following reasons:

- External hydrogen was used in the earlier work, while in the present case hydrogen generated *in-situ* by photocatalytic water splitting is used. Due to this reason activity observed in the present case is higher, in micromoles/g compared to nanomoles /g observed earlier.
- CO_2: H_2 mole ratio employed in earlier work is 0.177:1.67 m.moles. Due to the availability of excess hydrogen (but not in activated form) the rate of deactivation of the catalyst is much less. In the present case, CO_2 is employed in excess and CO_2: water

mole ration is 1: 0.038. Hence catalyst deactivation is severe due to limited availability of hydrogen via water splitting.

- Carrying out the reaction with suitable CO_2: H_2 mole ratio by increasing the partial pressure of water (or decreasing that of CO_2) could help to increase conversion and improve catalyst stability
- As pointed out in the earlier section, compositional changes in terms of substituting divalent and trivalent ions could lead to a number of potentially active catalysts that may display higher activity.
- Evaluation of catalysts in aqueous phase along with detailed analysis of liquid samples and for hydrogen, oxygen and CO in gas phase are to be carried out to get a complete product profile.

CHAPTER 5

SUMMARY & CONCLUSION

- The objective of the project was to explore the application of layered double hydroxides (LDH) or synthetic hydrotalcites of general formula $[M_3^{II} N^{III}(OH)_8]_2 CO_3^{2-}$(where M= Cu, Zn, Ni & N=Al, Ga, In & Fe) as catalysts for photocatalytic reduction of CO_2 with water. Earlier studies on similar systems, consisting of M= Zn, Cu & N= Al or Ga, had displayed measurable conversion (in terms of nano moles) of CO_2 to CO & methanol using UV-Visible light and external hydrogen as reductant.
- A host of LDH compounds with numerous combinations of divalent and trivalent metals and active interlayers of water & CO_3^{2-} with well-established structures are possible.
- Such LDH compounds are typical semi-conductors that possess valence and conductance band energy levels suitable for activation by UV Visible as well as normal solar radiation. Hence it was of interest to explore their use as photo catalysts for a number of conversions, especially for photo reduction of $CO_2$with water.
- In the present work, a total of six different LDH catalysts, three ternary systems consisting of Zn-Cu-Al, Zn-Cu-Ga and Zn-Cu-In and three quaternary systems consisting of Zn-Cu-[Al-In], Zn-Cu-[Al-Fe] and [Zn-Ni]-Cu-Al were considered for investigation as catalysts for CO_2 photo reduction brought out by active hydrogen generated by simultaneous water splitting process
- All the six catalysts were prepared from mixtures of respective nitrates by co-precipitation adopting the procedure reported in literature and subjected to characterization by XRD, FT-IR, UV-Vis, DRS and SEM techniques, which established the LDH structure.
- Photo catalytic reduction of CO_2 on these catalysts with water as the source of hydrogen was studied, using UV-Visible light source (300-700 nm).
- Reactions in batch mode were carried out in aqueous phase (by dispersion of catalyst in 0.2M aqueous NaOH) and vapour phase with CO_2 gas saturated with water vapour.
- Methanol, ethanol and acetaldehyde were the major products observed in all cases. Though methane and ethane were identified they could not be quantified.

- There is noticeable change in the product profile in both phases. Methanol and ethanol with very little amount of acetaldehyde are formed in aqueous phase, while only methanol and acetaldehyde are observed in vapour phase. Ethanol is not observed in vapour phase. Besides, the total amount of hydrocarbons formed in aqueous phase is higher than that in vapour phase.
- This difference in the reactivity and the product profile in two phases is due to the availability of the reducing agent, hydrogen. In aqueous phase availability of water in excess ensures higher hydrogen production by water splitting and hence reduction of CO_2 could proceed upto ethanol stage. In the vapour phase CO_2 is in excess and availability of hydrogen is less and hence reduction stops at acetaldehyde stage. For the same reason, overall conversion in aqueous phase is higher.
- Of all the catalysts, [Zn-Ni]-Cu-Al system displayed maximum activity and good stability in vapour phase reaction, yielding ~300 micro moles of methanol/ gram of the catalyst.
- Based on the quantity of methanol formed per gram of the catalyst in vapour phase, the activity of the LDH catalysts decreases in the following order:

  Zn-Cu-In< Zn-Cu-[Al-In]< Zn-Cu-[Al-Fe]< Zn-Cu-Al< Zn-Cu-Ga< [Zn-Ni] -Cu-Al
- Substitution of the divalent Zn by Ni brings about substantial increase in the overall activity for CO_2 photo reduction.
- Substantial changes in the band gap values observed for various hydrotacilte samples (Table.2) could be one of the reasons for the observed differences in the activity. Shifting of light absorption edge towards visible range would increase the activity with visible light.
- In the case of [Zn-Ni] –Cu-Al very small particle size could be an additional factor for the observed increase in activity.
- For many photo catalysts based on perovskite/pyrochlore structure, NiO is identified as highly efficient co-catalyst. The mechanism of promotion by Ni in this case is to be investigated further.
- In this context, it is worth exploring the whole range of compositions from Zn-Cu-Al to Ni-Cu-Al and also the incorporation of Ni in Zn-Cu-Ga system.

- Though the band gap for Zn-Cu-[Al-Fe] is less, its amorphous nature and larger crystallite size may adversely affect the activity.
- In the case of In based hydrotalcites, presence of free $In(OH)_3$ as additional phase as observed in XRD patterns could affect the performance.
- An in-house designed solar reactor was used to carry out CO_2 photo reduction in vapour phase on P-25, Ag/P-25 & CuO/P-25 catalysts using sun light as source of energy
- While all the three major products methanol, ethanol and acetaldehyde are observed with all catalysts. CO_2 conversions are low, possibly due to very low partial pressure of water. Maximum conversion is realized with P-25. After about 3-4 hours, the activity of the catalyst is reduced drastically.
- Increasing the partial pressure of water and conducting experiments in aqueous phase would increase the CO_2 reduction.
- External hydrogen was used in the earlier work, while in the present case hydrogen generated *in-situ* by photo catalytic water splitting is used. Due to this reason activity observed in the present case is higher, in micromoles/g compared to nano moles /g observed earlier.
- CO_2: H_2 mole ratio employed in earlier work is 0.177:1.67 m.moles. Due to the availability of excess hydrogen (but not in activated form) the rate of deactivation of the catalyst is much less. In the present case, CO_2 is employed in excess and CO_2: water mole ration is 1:0.038. Hence catalyst deactivation is severe due to limited availability of hydrogen via water splitting
- Carrying out the reaction with suitable CO_2: H_2 mole ratio by increasing the partial pressure of water (or decreasing that of CO_2) could help to increase conversion and improve catalyst stability.
- As pointed out in the earlier section, compositional changes in terms of substituting divalent and trivalent ions could lead to a number of potentially active catalysts that may display higher activity.
- Evaluation of catalysts in aqueous phase along with detailed analysis of liquid samples and for hydrogen, oxygen and CO in gas phase are to be carried out to get a complete product profile.

REFERENCES

1) **Ahmed , Y.Shibata , T.Taniguchi and Y Izumi** (2011) Journal of Catalysis **279** 123.
2) **Akira Fujishimaa, Xintong Zhanga, Donald. A. Trykb** (2007): Heterogeneous photocatalysis. International Journal of Hydrogen Energy **32** 2664 – 2672.
3) **Adachi, K.; Ohta, K.; Mijuma, T** (1994); *Sol. Energy*, ***53***, 187–190.
4) **Anpo, M.; Yamashita, H.; Ichihashi, Y.; Fujii, Y.; Honda, M.** (1997); *J.Phys. Chem. B*, **101**, 2632–2636.
5) **Bandi, A.; Kuhne, H. M. J**. (1992) Electrochem.Soc., **139**, 1605.
6) **Balzani, V.; Juris, A.; Venturi, M.** (1996) Chem. Rev.**, 96**, 759.
7) **Bandi, A. J**. (1990),Electrochem. Soc., 137, 2157.
8) **Collin, J.-P.; Harriman, A.; Heitz, V.; Odobel, F.; Sawage, J.-P. J**. (1994) Am. Chem. Soc., **116**, 5679.
9) **Cook, R. L.; Macduff, R. C.; Sammells, A. F.** (1988); *J. Electrochem. Soc.*, ***135***, 3069–3070.
10) **Etheridge, D. M.; Steele, L. P.; Langenfelds, R. L.; Francey, R. J.; Barnola, J.-M.; Morgan,** (2008), V. I. Historical CO_2 record form the Law Dome DE08, DE08-2, and DSS ice cores (atmospheric CO_2 concentrations, Antartic ice cores), Carbon Dioxide Information Center.
11) **Freund, H.-J.; Roberts, M. W. Surf (1996)**. Sci. Rep., **25**, 225-273.
12) **František Kovanda, Eva Káfuòková, Tomáš Rojka, Kamil Lang** (2008); Materials Structure, vol. **15**, no. 1.
13) **Green, D. W.; Perry** (2008), R. H. Perry's Chemical Engineers' Handbook; 8th ed.; McGraw-Hill**.**
14) **Halmann, M.; Ulman, M.; Blajeni, B. A**. (1983); *Sol. Energy*, ***31***, 429–431.
15) **Hori, Y. K., K.; Suzuki**, (1985). Chem. Lett., **11**, 1695.
16) **Hara, K.; Kudo, A.; Sakata, T.; Watanabe, M.** (1995) J. Electrochem.Soc., **142**, L57.
17) http://www.sc.doe.gov/bes/reports/files/SEU_rpt.pdf.
18) **Indrakanti, V. P., Kubicki, J. D. & Schobert, H.** (2009); *Energy Environ .Sci.* **2**, 745–758.
19) **Inoue, T.; Fujishima, A.; Konishi, S.; Honda, K**. (1979); *Nature*, ***277***, 637–638.
20) **Ikeue, K.; Nozaki, S.; Ogawa, M.; Anpo, M.** (2002) ; *Catal. Lett.*, ***80***, 111–114.

21) **J.C.S. Wu**, (2009). Cata. Surv.Asia**, 13**,30

22) **Kannan** (2006) ; Catalysis Surveys from Asia, Vol. **10,** Nos. 3/4, December.

23) **K. Takehiraa, and T. Shishidob** (2007); Catalysis Surveys from Asia, Vol. **11**, Nos. 1/2, June.

24) **Kazuhito, Hashimoto, Hiroshi Irie and Akira Fujishima** (2005); Journal of Applied Physics Vol. **44**, No. 12, pp. 8269–8285.

25) **Lo, C. C.; Hung, C. H.; Yuan, C. S.; Wu, J. F**. (2007) ; *Sol. Energy Mater. Sol. Cells **91***, 1765–1774.

26) **Lehn, J.-M.; Ziessel, R.** (1982) *Proc. Natl. Acad. Sci. U.S.A*, ***79***, 701–704.

27) **Marland, G.; Boden, T. A.; Andres, R. J.** (2005) Global, Regional, and National CO_2 Emissions, Carbon Dioxide Information Analysis Center, Oak Ridge National Laboratory, U.S. Department of Energy,.

28) **Russell, P. G. K., N.; Srinivasan, S.; Steinberg, M. (1977)** J. Electrochem.Soc., **124**, 1329.

29) **Rowan J. Braham and Andrew T. Harris** (2009) *Ind. Eng. Chem. Res.***, *48,*** 8890–8905.

30) **Song, C.** (2006) Cat.Today, 115, **2**.

31) **Schwartz, M. C.;Cook,R. L.; Kehoe, V. M.; Macduff, R. C.; Patel, J.; Sammells,** (1993) A . F. J. Electrochem. Soc., **140**, 614.

32) **Sayama, K.; Arakawa, H.** (1993); *J. Phys. Chem.*, ***97***, 531–533.

33) **Thampi, K. R.; Kiwi, J.; Graetzel,** (1987), M. *Nature **327***, 506–508.

34) **T. Inoue, A. Fujishima, S. Konishi, K. Honda**, (1979) Nature **277** 637-638.

35) **Tan, S. S.; Zou, L.; Hu, E**. (2007); *Sci. Technol. Adv. Mater.*, ***9***, 89–92.

36) **Varghese, O. K.; Paulose, M.; LaTempa, T. J.; Grimes, C.** (2009) A. *Nano Lett. **9***, 731–737.

37) **Walther, D.; Ruben, M.; Rau, S.** (1999) Coordi.Chem. Rev., **182**, 67.

38) **Wu, J. C. S.; Wu, T.-H.; Chu, T.; Huang, H.; Tsai, D.** (2008) *Top. Catal. **47***, 131–136.

39) **Wang, C.; Thompson, R. L.; Baltrus, J.; Matranga, C.** (2010) *J. Phys. Chem. Lett.*, ***1***, 48–53.

40) **Xiaoding, X.; Moulijn, J.** (1996) A. Energy & Fuels **10**, 305.

41) **Xia, X-H,; Jia, Z.-J.; Yu, Y.; Liang, Y.; Wang, Z.** (2007); Ma, L.-L. *Carbon*, ***45***, 717–721.